



**HAL**  
open science

## Dissecting the membrane lipid binding properties and lipase activity of *Mycobacterium tuberculosis* LipY domains

Pierre Santucci, Nabil Smichi, Sadia Diomandé, Isabelle Poncin, Vanessa Point, Hélène Gaussier, Jean-François Cavalier, Laurent Kremer, Stéphane Canaan

► **To cite this version:**

Pierre Santucci, Nabil Smichi, Sadia Diomandé, Isabelle Poncin, Vanessa Point, et al.. Dissecting the membrane lipid binding properties and lipase activity of *Mycobacterium tuberculosis* LipY domains. FEBS Journal, 2019, 10.1111/febs.14864 . hal-02137694

**HAL Id: hal-02137694**

**<https://amu.hal.science/hal-02137694>**

Submitted on 29 Jan 2020

**HAL** is a multi-disciplinary open access archive for the deposit and dissemination of scientific research documents, whether they are published or not. The documents may come from teaching and research institutions in France or abroad, or from public or private research centers.

L'archive ouverte pluridisciplinaire **HAL**, est destinée au dépôt et à la diffusion de documents scientifiques de niveau recherche, publiés ou non, émanant des établissements d'enseignement et de recherche français ou étrangers, des laboratoires publics ou privés.

1           **Dissecting the membrane lipid binding properties and lipase activity of the**  
2                                   ***Mycobacterium tuberculosis* LipY domains**

3  
4 Pierre Santucci<sup>§</sup>, Nabil Smichi<sup>§</sup>, Sadia Diomandé<sup>§</sup>, Isabelle Poncin<sup>§</sup>, Vanessa Point<sup>§</sup>, Hélène  
5 Gaussier<sup>+</sup>, Jean-François Cavalier<sup>§</sup>, Laurent Kremer<sup>#,†</sup> and Stéphane Canaan<sup>§\*</sup>

6  
7 <sup>§</sup>Aix-Marseille Univ, CNRS, LISM, IMM FR3479, Marseille, France.

8 <sup>+</sup>Aix Marseille Univ, Université de Toulon, CNRS, IRD, MIO, Marseille, France

9 <sup>#</sup>Institut de Recherche en Infectiologie de Montpellier (IRIM), Université de Montpellier, CNRS  
10 UMR9004, Montpellier, France.

11 <sup>†</sup>INSERM, IRIM, Montpellier, France.

12  
13 **\*Corresponding author:**

14 Stéphane Canaan, e-mail: [canaan@imm.cnrs.fr](mailto:canaan@imm.cnrs.fr), Tel: + 33 (0)491164093.

15  
16 **Running title:** Interactions between LipY domains and membrane lipids

17  
18 **Keywords:** *Mycobacteria*, lipolytic enzyme, triacylglycerol, Interaction DOPG-protein, FTIR  
19 spectroscopy, monomolecular film.

21 **ABSTRACT**

22 The *Mycobacterium tuberculosis* LipY protein, a prototype of the proline-glutamic acid (PE) family,  
23 exhibits a triacylglycerol (TAG) hydrolase activity that contributes to host cell-lipid degradation and  
24 persistence of the bacilli. LipY is found either as a full-length intracytosolic form or as a mature  
25 extracellular form lacking the N-terminal PE domain. Even though the contribution of the  
26 extracellular form in TAG consumption has been partly elucidated, very little information is available  
27 regarding the potential interactions of each form of LipY with either the cytoplasmic membrane for  
28 the full-length protein or with the outer membrane for the matured form. Herein, several LipY  
29 variants truncated in their N-terminal domain were produced and biochemically characterized in  
30 lipid-protein interaction assays using the monomolecular film technique and Fourier transform  
31 infrared spectroscopy. Comparison of the catalytic activities of these recombinant proteins showed  
32 that LipY $\Delta$ 149, corresponding to the extracellular form of LipY lacking the PE domain, is more  
33 active than the full-length protein. This confirms previous studies reporting that the PE domain  
34 negatively modulates the TAG hydrolase activity of LipY. Lipid-protein interaction studies indicate  
35 that the PE domain anchors LipY onto membrane lipids. Consistent with these findings, LipY $\Delta$ 149  
36 was loosely-associated with the mycobacterial cell wall and that this interaction is mediated by the  
37 sole lipase domain. Altogether, our results bring new information regarding the molecular  
38 mechanisms by which LipY either binds and hydrolyzes host cell lipids or degrades TAG, the major  
39 source of lipids within mycobacterial intracytosolic lipid inclusions.

40

## 41 INTRODUCTION

42 Tuberculosis (TB), which is caused by the highly versatile pathogenic agent *Mycobacterium*  
43 *tuberculosis* (*Mtb*), remains an important global health issue with more than 10 million new cases  
44 and approximately 1.6 million deaths in 2017 [1]. Upon infection, *Mtb* uses several strategies to avoid  
45 and/or resist a wide range of microbicidal processes of immune cells. It can also persist for extensive  
46 periods of time within granulomas, resulting in a clinically asymptomatic latent tuberculosis infection  
47 (LTBI) [2, 3]. It is estimated that around two billion individuals are latently infected worldwide,  
48 providing a major reservoir for *Mtb* [1]. Our understanding of the processes leading to LTBI  
49 establishment and reactivation at the molecular and cellular levels, remains an outstanding challenge  
50 for the scientific community and a crucial step for a better control of the disease [4]. It is assumed  
51 that *Mtb*'s survival processes rely mainly on a very dynamic metabolic realignment within the  
52 granuloma microenvironment, where *Mtb* preferentially uses fatty acids (FFA) as a carbon source  
53 during long-term infections [5-9]. Several studies demonstrated that pathogenic mycobacteria can  
54 utilize host-derived FFA to build up their own intracytosolic lipid inclusions (ILI), which will be  
55 further used as a source of nutrient [10-14]. The exact role of these neutral lipid-rich structures in  
56 mycobacterial pathogenesis remains elusive, but it has been proposed that ILI may promote *Mtb*  
57 survival and persistence *in vivo* [8, 10, 11, 15]. However, the molecular bases of the dynamics of FFA  
58 acquisition and storage remain poorly understood [16].

59 *Mtb* contains two specific families of proteins, designated PE and PPE proteins [17, 18], and while  
60 the PE proteins possess a conserved N-terminal domain of about 100 amino acids typified by a Pro-  
61 Glu signature motif, the PPE proteins possess a 180 amino acids N-terminal domain characterized by  
62 a Pro-Pro-Glu signature [19-21]. Due to their abundance in pathogenic mycobacteria, it has been  
63 postulated that PE and PPE proteins play important functions in mycobacterial survival and  
64 pathogenesis. Nevertheless, the real function of these proteins remains to be elucidated [21-23].  
65 Several studies emphasized the participation of the PE domain in protein translocation, an event very  
66 likely to be mediated by the type VII secretion system ESX-5 [24-27]. Among the PE members,

67 Rv3097c, also known as LipY, is a 437 amino acids protein belonging to the Hormone-Sensitive  
68 Lipase family (HSL) possessing a C-terminal lipase domain [28-30]. Deb *et al.*, (2006) demonstrated  
69 that LipY is a true triacylglycerol (TAG) lipase involved in intracellular TAG hydrolysis in *Mtb* upon  
70 carbon deprivation [29]. Moreover, a *Mtb lipY*-deficient mutant failed to escape from dormancy in an  
71 *in vitro* granuloma model [31]. Together, these results point out to LipY as an essential factor required  
72 for intracytosolic lipid catabolism and exit from a dormancy state. Subsequent work described that  
73 the dual location of LipY in mycobacteria and its secretion rely both on a well-defined sequence of  
74 events by the ESX-5 pathway [25]. The consensus YxxxD/E motif within the PE domain allows the  
75 recognition/translocation by the ESX-5 machinery. The protein is subsequently cleaved by the MycP5  
76 protease within the linker region between Gly<sup>149</sup> and Ala<sup>150</sup>, leading to the formation of an N-terminal  
77 truncated form associated with the mycobacterial cell surface [25]. In *M. marinum* LipY, the PE  
78 domain is substituted by a PPE domain [28] and the presence of this surface-exposed mature LipY  
79 strongly increases its TAG hydrolase activity [25]. Recently, we have demonstrated that a *M. bovis*  
80 BCG  $\Delta lipY$  mutant is impaired in ILI formation within foamy macrophages, suggesting that LipY is  
81 an essential factor involved in host-derived TAG consumption [14]. Additional biochemical data  
82 indicated that LipY lacking its PE domain expresses increased TAG-hydrolase activity *in vitro* [28],  
83 suggesting that the PE domain acts as a modulator of the catalytic activity [14, 28]. Collectively, these  
84 findings imply that LipY plays a central role in TAG metabolism during the *Mtb* life cycle by  
85 participating in the hydrolytic processes of both extracellular and intracellular lipids. Nevertheless,  
86 little is known about the biochemical properties at the molecular level of the various forms of LipY  
87 as well as their respective contribution in hydrolysis of extracellular TAG contained in LB and/or  
88 intracellular TAG contained in ILI.

89 In this study, the shortest domain of LipY exerting hydrolytic activity has been defined and several  
90 recombinant variants of LipY have been characterized. We thus examined the ability of these proteins  
91 to interact with membranes using Langmuir monolayers as an *in vitro* model of cell membranes along  
92 with Fourier Transform InfraRed (FTIR) spectroscopy. Langmuir monolayers consisting of

93 supramolecular lipid films formed at an air-buffer interface are mimicking biological membranes and  
94 represent attractive membrane models [32] particularly suited to study membrane-protein interactions  
95 [33-37]. Fourier Transform InfraRed (FTIR) spectroscopy, performed in parallel to Langmuir  
96 monolayers, is a suitable technique to investigate the lipid membrane physical states (*i.e.*, chain  
97 ordering, phase transition) occurring in presence of a protein [38-40].

98 Phosphatidylglycerol being the most abundant glycerophospholipid found in mycobacteria [41-  
99 43], 1,2-dioleoyl-*sn*-glycero-3-phosphoglycerol (DOPG) is often chosen as model phospholipid  
100 interfacial experiments. Therefore, combining both techniques can provide crucial information  
101 regarding interactions of protein with either the cytoplasmic or the outer membrane. In addition, in  
102 order to link their potential physiological roles *in vivo*, a set of LipY variants were either  
103 overproduced in lipid-rich persistent-like *M. smegmatis*, or in *M. marinum* which allows a  
104 constitutive translocation of these effectors through the ESX-5 machinery. Both mycobacteria were  
105 used as tools for establishing the respective role of the PE, linker and lipase domains in the  
106 translocation and maturation processes, thereby yielding essential information regarding the  
107 hydrolytic mechanisms of intra- as well as extracellular TAG.

## 108 RESULTS AND DISCUSSION

### 109 Expression and biochemical characterization of LipY and its truncated versions.

110 LipY is either found in the mycobacterial cytoplasm where it hydrolyzes ILI [29] or translocated  
111 *via* ESX-5 to the bacterial surface, where, upon cleavage of the N-terminal PE domain, the mature  
112 enzyme can interact and hydrolyze the host cell lipids [14, 25]. The contribution of the various LipY  
113 domains in its interfacial activity has, however, not yet been explored. To provide insights into their  
114 specific biological functions, we first generated LipY $\Delta$ PE, LipY $\Delta$ 149 and LipY $\Delta$ 170 truncated  
115 forms, by *i*) removing the PE domain (LipY $\Delta$ PE; lacking the first 97 residues), *ii*) deleting the first  
116 149 residues (LipY $\Delta$ 149; the mature form exposed to the mycobacterial cell wall surface) and *iii*) by  
117 further shortening the protein towards the C-terminus (LipY $\Delta$ 170; consisting essentially of the C-  
118 terminal catalytic domain), respectively (**Figure 1A**). All genes, including full-length *lipY*, were  
119 cloned into the pSD26 and fused to a 6 $\times$ His-tag encoding sequence and used to transform the  
120 *M. smegmatis* mc<sup>2</sup>155 *groEL1* $\Delta$ C strain [44, 45]. Following induction with acetamide, cultures were  
121 harvested and the recombinant proteins were purified using Ni<sup>2+</sup>-charged immobilized metal affinity  
122 chromatography, yielding 15-20 mg of protein per L of culture. Following size exclusion  
123 chromatography, the purity of each protein was subsequently analyzed by SDS-PAGE gel (**Figure**  
124 **1B**) and the nature of each protein was further confirmed by MALDI-TOF and N-terminal sequencing  
125 analyses (data not shown).

126 TAG with short, medium and long fatty acyl chains were used as substrates and assayed in the  
127 presence of each protein using the pH-stat technique [14, 46, 47]. As shown in **Figure 1C-D-E**, for  
128 each protein, the specific activity (SA) decreased gradually as a function of the lipid chain length.  
129 The removal of the first 170 residues did not affect the enzyme typoselectivity. LipY, LipY $\Delta$ PE,  
130 LipY $\Delta$ 149 and LipY $\Delta$ 170 hydrolyzed preferentially short-chain TAG (tributyrin) with a SA of around  
131  $119.0 \pm 11.1$ ,  $185.0 \pm 13.0$ ,  $215.0 \pm 24.0$  and  $75.0 \pm 6.0$  U/mg, respectively. Regardless of the  
132 substrate used, LipY $\Delta$ PE and LipY $\Delta$ 149 were up to 1.8 times more active than full-length LipY  
133 (**Figure 1F**). LipY $\Delta$ 170, the shortest LipY variant, exhibited SA of  $75.0 \pm 6.0$ ,  $16.0 \pm 2.0$  and 2.8

134  $\pm 0.1$  U/mg on tributyrin, trioctanoin and olive oil, respectively; and expressed the lowest activity as  
135 compared to the other proteins (**Figure 1C-D-E**). The SA of LipY $\Delta$ PE and LipY $\Delta$ 149 were  
136 comparable for tributyrin ( $185.0 \pm 13.0$  and  $215.0 \pm 24.0$  U/mg, respectively), trioctanoin ( $63.0 \pm 1.0$   
137 and  $55.0 \pm 5.0$  U/mg, respectively) and for long-chain triolein ( $5.2 \pm 0.2$  and  $6.3 \pm 0.1$  U/mg,  
138 respectively) used as substrates, suggesting that the first 53 residues of the linker motif had only a  
139 slight impact on LipY catalytic activity.

140 Moreover, since some lipases can also act as phospholipases, each LipY mutant form was also  
141 tested for their potential phospholipase A1 and A2 activities using a highly sensitive fluorescent-  
142 labeled phospholipid assay [43]. As anticipated and previously showed for LipY [43], none of the  
143 LipY truncated versions exhibited phospholipase activity.

144

#### 145 **Overexpression of LipY variants increased TAG consumption in *M. smegmatis* under lipid-rich** 146 **persistent-like conditions.**

147 It is well recognized that TAGs are major lipid storage molecules in bacteria belonging to the  
148 *Actinobacteria* phylum [48], including *Mycobacterium* [15, 49-52]. We recently showed that TAG  
149 accumulation under the form of ILI during infection in foamy macrophages was impaired when  
150 constitutively overproducing the cytoplasmic LipY $\Delta$ PE in *M. bovis* BCG. These effects were neither  
151 observed with the full length protein nor with the catalytically-inactive mutant (LipY $\Delta$ PE<sup>S309A</sup>),  
152 supporting that the PE domain is directly influencing the activity of LipY towards both mycobacterial  
153 and host-derived TAGs [14, 28]. To gain additional insight and confirm our previous biochemical  
154 results, we investigated here the effect of the PE domain and the linker region with respect to lipase  
155 activity *in vivo*. *M. smegmatis* recombinant strains harboring either the empty pSD26 vector,  
156 pSD26::*lipY*, pSD26::*lipY* $\Delta$ PE, pSD26::*lipY* $\Delta$ 149 or pSD26::*lipY* $\Delta$ 170 were grown for 48 h in a  
157 well-defined carbon rich/nitrogen limiting medium that promotes the induction of heavily lipid-  
158 loaded mycobacteria [53]. Cultures were harvested and re-suspended in a mineral salt medium devoid  
159 of glycerol but supplemented with 0.2% (w/v) acetamide to trigger catabolic reprogramming [53] and

160 the production of the respective LipY recombinant forms. Bacteria were collected at two distinct time  
161 points (*i.e.* 6 h and 12 h), and lyophilized prior to apolar lipid extractions and thin layer  
162 chromatography (TLC) for lipid profile analysis. As shown in **Figure 2A**, the overproduction of LipY  
163 and its variants significantly reduced the intracellular pool of TAG by 37-51% after 6 h and up to  
164 69% after 12 h, in comparison with the control strain carrying the empty vector. In each case,  
165 LipY $\Delta$ PE and LipY $\Delta$ 149 were the most active forms *in vivo*, leading to respectively 26.4% and 19.0%  
166 relative TAG levels, *vs.* a mean value of  $36.0 \pm 3.2\%$  for LipY and LipY $\Delta$ 170 after 12 h of induction.  
167 These results are consistent with our biochemical data and with previous studies using either  
168 genetically-modified *M. smegmatis* pSD26::*lipY* and *M. smegmatis* pSD26::*lipY* $\Delta$ PE [28] or *M. bovis*  
169 BCG pMV261::*lipY* and *M. bovis* BCG pMV261::*lipY* $\Delta$ PE strains [14, 28].

170 To gain further insight into this molecular mechanism, 3D structural models were generated using  
171 the I-TASSER server. As proposed previously [14, 54], the N-terminal PE domain could be easily  
172 distinguished from the C-terminal domain and is composed of four  $\alpha$ -helices ( $\alpha$ 1 to  $\alpha$ 4) (**Figure 2B**  
173 – highlighted in blue) [14, 54]. Comparison of the LipY and LipY $\Delta$ PE models [14] suggests that the  
174 four  $\alpha$ -helices of the PE domain cover the active site of the enzyme. This steric hindrance may be  
175 responsible for a reduced substrate accessibility and for the lower catalytic activity of the full-length  
176 protein, as previously proposed [14, 28, 55]. Concerning the linker motif, this 53 amino acid region  
177 comprises three  $\alpha$ -helices (**Figure 2B-C** – highlighted in green). From its location, this region is very  
178 likely to be extremely flexible, hence unable to induce a steric barrier masking the catalytic site. The  
179 3D model of LipY $\Delta$ 149 displays a similar “open” active site (**Figure 2D**). These observations are in  
180 agreement with the biochemical data. In contrast, amputation of the next 21 amino acids in  
181 LipY $\Delta$ 149, yielding LipY $\Delta$ 170 (**Figure 2D** – highlighted in orange; and **Figure 2E**) triggers a sharp  
182 drop in the lipase activity (**Figure 1F**). Since this deletion occurs directly in a  $\alpha$ -helix, one can  
183 speculate it would lead to severe conformational alterations affecting catalysis.

184 From these results, it could be inferred that the increased activity shared by LipY $\Delta$ PE and  
185 LipY $\Delta$ 149, as compared to LipY, would result from a better accessibility and/or recognition of the

186 lipid to the active site, due to the absence of the PE domain. In addition, the 21 first amino acid  
187 residues of the linker region in LipY $\Delta$ 149 (**Figure 2D-E**) seem to be essential for the enzyme activity,  
188 possibly by stabilizing this extracellular mature form in a suitable conformation within the cell wall  
189 and during TAG hydrolysis, as previously proposed [14, 28, 55].

190

### 191 **Interactions and binding capacity of LipY and its truncated forms with model membrane lipids.**

192 To get additional elements regarding the anchoring process of LipY within biological membranes,  
193 we investigated how the LipY domains influence the adsorption capacity of the protein using the non-  
194 hydrolysable 1,2-dioleoyl-*sn*-glycero-3-phosphoglycerol (DOPG) monomolecular films.

195 This was achieved by measuring the interfacial binding properties of each LipY variant onto DOPG  
196 monolayers, first by determining the effect of initial surface pressure ( $\Pi_i$ ) on the interaction of the  
197 different protein forms with the monolayer. For this purpose, the increase in surface pressure ( $\Delta\Pi_{\max}$ ),  
198 directly reflecting the variation of DOPG molecular area (*i.e.* lipid packing) upon protein adsorption,  
199 was monitored immediately following protein injection at various  $\Pi_i$  values, ranging from 5 to around  
200 20 mN/m. The plot  $\Delta\Pi_{\max} = f(\Pi_i)$  depicted in **Figure 3A** allowed to evaluate the adsorption  
201 parameters of LipY and its derivatives onto DOPG monolayer. In all cases, the  $\Delta\Pi_{\max}$  was found to  
202 decrease linearly with the increase of  $\Pi_i$ . Linear extrapolation to zero surface pressure increase  
203 ( $\Delta\Pi_{\max} = 0$ ) allowed to estimate the critical surface pressure ( $\Pi_c$ ) [56] (also called “maximum  
204 insertion pressure” [57]) as being equal to  $22.5 \pm 1.2$ ,  $17.2 \pm 0.83$ ,  $16.4 \pm 0.49$  and  $14.3 \pm 0.25$  mN.m<sup>-1</sup>  
205 <sup>1</sup> for LipY, LipY $\Delta$ PE, LipY $\Delta$ 149 and LipY $\Delta$ 170 adsorbed onto DOPG film, respectively. Above  
206 these  $\Pi_c$  value, specifically related to the protein and the lipid forming the monolayer, no increase in  
207 the surface pressure occurred [56]. The full-length protein appeared as the most tensioactive form  
208 binding to DOPG monolayers, followed by LipY $\Delta$ PE and LipY $\Delta$ 149, while LipY $\Delta$ 170 poorly  
209 adsorbed onto the phospholipid membrane. It appears that the ranking in the penetration capacity  
210 (*i.e.*,  $\Pi_c$  values) of the four proteins is directly related to the size of the deletions.

211 The plots depicted in **Figure 3A** can also provide additional information regarding the binding  
212 parameters of these enzymes (**Table 2**), such as  $\Delta\Pi_0$  (y-intercept of the curves corresponding to  $\Pi_i =$   
213 0) and the synergy factor noted “ $a$ ” (slope of the linear regression + 1) introduced by Salesse’s group  
214 [58-60], where a positive “ $a$ ” value is linked to favorable binding of the protein and the  $\Pi_c$  represents  
215 an insertion surface pressure. In contrast, a negative synergy factor correlates with unfavorable  
216 binding of a protein to a phospholipid monolayer whereas the associated  $\Pi_c$  corresponds to an  
217 exclusion surface pressure. Finally, an “ $a$ ” value close to zero corresponds to a stationary state where  
218 the binding of the protein is neither favored nor disfavored by the lipid monolayer.

219 Based on these rules, the positive value of the synergy factor ( $+0.113 \pm 0.010$ ) and the occurrence  
220 of a  $\Delta\Pi_0$  ( $20.0 \pm 1.1 \text{ mN.m}^{-1}$ ) lower than the related  $\Pi_c$  ( $22.5 \pm 1.2 \text{ mN.m}^{-1}$ ) observed for LipY was  
221 consistent with a high penetration capacity of LipY onto phospholipid films. In contrast, with  
222 LipY $\Delta$ 170 ( $a = -0.177 \pm 0.005$ ;  $\Delta\Pi_0 = 16.9 \pm 0.3 \text{ mN.m}^{-1}$ ) and LipY $\Delta$ PE ( $a = -0.564 \pm 0.043$ ;  $\Delta\Pi_0$   
223  $= 26.9 \pm 1.3 \text{ mN.m}^{-1}$ ), the negative  $a$  values and a  $\Delta\Pi_0$  larger than the corresponding  $\Pi_c$  were  
224 correlated with a repulsion of both enzymes as a function of the compactness of the monolayer.  
225 Regarding LipY $\Delta$ 149, a negative but almost close to zero synergy factor ( $-0.023 \pm 0.001$ ) was  
226 determined and the  $\Delta\Pi_0$  ( $16.8 \pm 0.5 \text{ mN.m}^{-1}$ ) was not significantly different from the  $\Pi_c$  value  
227 ( $16.4 \pm 0.49 \text{ mN.m}^{-1}$ ). These results reflect that the binding of LipY $\Delta$ 149 onto DOPG monolayer is  
228 neither favored nor disfavored. As a consequence, the decrease in the adsorption capacity of this  
229 protein may only be related to the reduction of the “free” area due to an increase in the lipid packing  
230 with the surface pressure [58, 60].

231 It can be inferred that, upon deletion of the PE domain and/or the linker unit, the proteins are  
232 excluded from the DOPG monolayer, in contrast to the full-length protein which retains the capacity  
233 to bind to phospholipid films. Thus, the PE domain may, presumably, favor the adsorption of LipY  
234 onto DOPG monolayers, thereby playing a key role in the penetration/binding of LipY to membranes.  
235 Conversely, cleavage of the N-terminus results in a mature protein that remains loosely attached to  
236 the cell wall, as proposed by Daleke *et al.* [25].

237 IR spectroscopy was subsequently used to study the protein to lipid interaction from a molecular  
238 point of view. Since lipid molecules are active in infrared (IR) through their hydrophobic [61],  
239 interfacial and polar head group [62], the molecular characterization of phospholipid assembly and  
240 phenomena affecting the behavior of the hydrophobic core of the lipid molecule [63-65] was followed  
241 in the presence or absence of the different proteins. Here, multilamellar liposomes of DOPG were  
242 used as a simple model for biomembranes and the conformational changes of lipids induced by the  
243 interaction of the acyl chain region with LipY and its mutants was monitored by analysis of the  
244 methylene stretching band vibration (**Figure 3B**). This region of IR spectra is indeed dominated by  
245 two main bands namely symmetric ( $\nu_s(\text{CH}_2)$ ) and antisymmetric ( $\nu_{as}(\text{CH}_2)$ ) methylene stretching  
246 located near 2850 and 2920  $\text{cm}^{-1}$ , respectively (data not shown). The thermotropism of lipid is  
247 characterized by a shift of the wavenumber of these stretching vibration bands, which are sensitive to  
248 the presence of gauche conformers [66-68], making them useful probes for following lipid phase  
249 transition and membrane fluidity. The **Figure 3B** displays the temperature dependence of  $\nu_{as}(\text{CH}_2)$   
250 vibration of the DOPG acyl chain in the absence and the presence of recombinant proteins. According  
251 to the literature, the transition temperature ( $T_m$ ) for pure DOPG is  $-18^\circ\text{C}$  [69, 70]; therefore all  
252 experiments were carried out in the DOPG liquid-crystalline phase. All the wavenumbers of  $\nu_{as}(\text{CH}_2)$   
253 mode from 27 to  $40^\circ\text{C}$  were lower in the presence of each protein form in comparison to the pure  
254 lipid, indicating that all the proteins studied altered the acyl chain conformation. These changes have  
255 been attributed to the presence of hydrophobic protein segments within the hydrophobic core of lipid  
256 membranes increasing the steric hindrance and therefore decreasing the membrane flexibility [71,  
257 72]. However, while the differences of the  $\nu_{as}(\text{CH}_2)$  of the lipid alone and in the presence of each  
258 protein was significant, the impact of each protein on the conformational change of the acyl chains  
259 was difficult to quantify. Above  $40^\circ\text{C}$ , the wavenumber of the  $\nu_{as}(\text{CH}_2)$  mode in the presence of LipY  
260 was still below the wavenumber of the lipid alone, meaning that the protein was still interacting with  
261 the acyl chains of lipid membranes, while the effect of the LipY mutant forms (LipY $\Delta$ PE, LipY $\Delta$ 149  
262 and LipY $\Delta$ 170) was less obvious. This suggests that LipY strongly interacts with the lipid chains

263 while this interaction is weaker for the mutants. Thus, regardless of the temperature, LipY induces a  
264 stronger conformational change in the lipid acyl chains, than the different mutants, suggesting that  
265 the presence of the PE domain enhanced the insertion within the hydrophobic core of the bilayers  
266 while the extracellular LipY $\Delta$ 149 is weakly anchored to DOPG liposome. Overall, these results are  
267 in agreement with those obtained using DOPG monomolecular films.

268

### 269 **Translocation through ESX-5 and anchoring investigations of LipY and its truncated forms *in*** 270 ***vivo*.**

271 Mycobacteria belonging to the *M. tuberculosis* complex express LipY in infected cells but are  
272 unable to do so when growing *in vitro* under standard laboratory conditions [25, 28]. Furthermore,  
273 *M. smegmatis* lacks an ESX-5 secretion system. Thus, to further delineate LipY processing and  
274 anchoring to the mycobacterial cell wall, studies were done in *M. marinum*, which is able to  
275 translocate and mature LipY through the ESX-5 secretion machinery [25]. To achieve this goal,  
276 pVV16-based constructs allowing the constitutive expression of the *lipY* truncated versions fused to  
277 a C-terminal His-tag (**Figure 4A**) were generated. The corresponding *M. marinum* strains were grown  
278 and bacterial pellets subjected to detergent extraction using Genapol<sup>®</sup>-X080, a powerful non-ionic  
279 detergent which allows to solubilize proteins that are localized within the capsule and the  
280 mycomembrane without impacting the cytoplasmic membrane (CM), the peptidoglycan (PG) or  
281 arabinogalactan (AG) fractions [25, 27, 73-75]. Proteins were then revealed by immunoblotting using  
282 a HisProbe<sup>™</sup> HRP conjugate [25] (**Figure 4B-C**). As expected, two immunoreactive bands were  
283 detected in the strain harboring pVV16::*lipY*, corresponding to the mature (black arrow) and  
284 cytoplasmic forms (grey arrows) (**Figure 4C** – upper panel). When cells were treated with Genapol<sup>®</sup>-  
285 X080, the mature protein was only detected in the surface-exposed fraction, demonstrating that  
286 translocation and maturation occurred. Two other variants, LipY $\Delta$ 149 and LipY<sup>E92A</sup> (carrying a point  
287 mutation within the YxxxD/E consensus secretion signal abrogated maturation and secretion of the  
288 protein) were also included as cytoplasmic controls [25, 26] (**Figure 4B**). LipY maturation catalyzed

289 by the MycP5 protease occurred at a specific site between Ser<sup>148</sup>, Gly<sup>149</sup> and Ala<sup>150</sup> [25]. However,  
290 that point mutations at each of these three residues failed to abolish maturation and secretion of the  
291 protein suggested alternative cleavage sites [25]. Our results, using a LipY<sup>G149D</sup> mutant, support the  
292 findings by Daleke *et al.* [25] (**Figure 4C**).

293 Overall, these data prompted us to investigate the contribution of the linker domain in both  
294 translocation and anchoring processes and to define whether the S<sup>148</sup>GA<sup>150</sup> motif and the linker  
295 domain were required for maturation and surface localization of the protein in *M. marinum*.

296 Therefore, two additional LipY mutated proteins were constructed by fusion of the PE domain to the  
297 S<sup>148</sup>GA<sup>150</sup> motif to retain the putative proteolytic site and by deleting: *i*) either the 51 residues of the  
298 linker motif to generate a PE-SGA-LipY $\Delta$ 149 recombinant protein; or *ii*) the entire linker motif thus  
299 producing the PE-SGA-LipY $\Delta$ 170 chimera (**Figure 4A**). In both cases, the chimeric proteins PE-  
300 SGA-LipY $\Delta$ 149 and PE-SGA-LipY $\Delta$ 170 were translocated and found anchored to the mycobacterial  
301 surface (**Figure 4C**). Interestingly, a single band of approximately 30 kDa was detectable for the PE-  
302 SGA-LipY $\Delta$ 149 variant, suggesting that the cleavage may have occurred, as for a WT protein, at the  
303 G<sup>149</sup>A<sup>150</sup> position. In contrast, concerning the PE-SGA-LipY $\Delta$ 170-expressing strain, two distinct  
304 bands of lower molecular weights (~ 26-28 kDa) were detected, suggesting two different cleavage  
305 sites (**Figure 4C**). To precisely define these cleavage sites, *M. marinum* displaying the pVV16::PE-  
306 SGA-lipY $\Delta$ 170 was treated with Genapol<sup>®</sup>-X080. The supernatant containing the cell wall-associated  
307 proteins was then loaded onto a Ni<sup>2+</sup> NTA affinity column to purify the 6 $\times$ His-tagged proteins. Using  
308 this approach, a single and pure band of approximately 28 kDa, highly reactive with the 6 $\times$ HisProbe,  
309 was detected (**Figure 4D**). Despite several attempts, we, however, failed to co-purify the second band  
310 with a lower molecular weight. N-terminal sequencing by using Edman degradation on pure fractions  
311 containing the 28 kDa band identified a protein cleaved just after the S<sup>148</sup>GA<sup>150</sup> motif, thus leading  
312 to the sole lipase domain starting at the sequence E<sup>171</sup>THFA. Interestingly, this mature LipY $\Delta$ 170  
313 form lacking the linker region was able to bind the mycobacterial cell wall, demonstrating, for the

314 first time, that if the linker domain does not seem to be essential for anchoring the protein to the  
315 mycomembrane, it remains crucial for full lipase activity (**Figure 1F**).

316

### 317 **Concluding remarks**

318 Understanding the physiological properties of lipid-rich persistent-like bacilli at both cellular and  
319 molecular levels, and more precisely how mycobacteria utilize host-derived lipids for building-up  
320 their own ILI is crucial. We show here that the secreted LipY $\Delta$ 149 protein was not only more active  
321 than its full-length cytoplasmic form (**Figure 5**), but was also essential for intraphagosomal-TAG  
322 breakdown, thus leading to lipid-rich persistent-like mycobacterial phenotype within foamy  
323 macrophages. Our biochemical characterization of several truncated forms of LipY confirmed that  
324 the N-terminal PE domain negatively affects the TAG hydrolase activity of the protein by generating  
325 a steric hindrance in the vicinity of the active site. By combining biochemical and biophysical  
326 approaches, we also demonstrate that the PE domain affects also the lipid binding activity onto  
327 phospholipid monolayers and liposomes (**Figure 5**). Both FTIR spectroscopy and monomolecular  
328 film experiments emphasized the PE-mediated anchoring capacity of LipY within phospholipids.  
329 Mycobacteria cell fractionation followed by immunoblotting strongly suggests that the linker region  
330 is dispensable for proper maturation and localization, but remains crucial for the enzymatic activity.  
331 Altogether, we provide compelling evidence that the PE domain as well as the linker region impact  
332 on the enzymatic properties of LipY by distinct molecular mechanisms, which are directly linked to  
333 its physiological substrates either host-derived or intracellular TAG in the form of ILIs (**Figure 5**).

## 334 **EXPERIMENTAL PROCEDURES**

### 335 **Bacterial strains and growth conditions**

336 *E. coli* DH10B cells (*Life technologies*, Saint Aubin, France) were grown at 37°C in Luria Bertani  
337 (LB) broth (*Euromedex*, Souffelweyersheim, France) or onto LB agar plates. Culture media were  
338 supplemented with 200 µg/mL hygromycin B or 50 µg/mL kanamycin (*Euromedex*,  
339 Souffelweyersheim, France). The *M. smegmatis* mc<sup>2</sup>155 *groEL1ΔC* strain [44] was usually grown at  
340 37°C under shaking (220 rpm) in complete Middlebrook 7H9 medium (*BD-Difco*) supplemented with  
341 0.05% Tween 80 (v/v), 0.2% glycerol (v/v), 0.5% bovine serum albumin (BSA) (w/v), 0.2% glucose  
342 (w/v). The *M. marinum* M strain [76] was grown at 32°C under shaking (220 rpm) in Middlebrook  
343 7H9 medium supplemented with 0.05% Tween 80 (v/v), 0.2% glycerol (v/v) and 10% oleic acid,  
344 albumin, dextrose, catalase (OADC enrichment; *BD-Difco*). Transformants were selected on  
345 Middlebrook 7H9 agar containing either 50 µg/mL hygromycin B or 50 µg/mL kanamycin. Plates  
346 were incubated at 37°C for 3-5 days for *M. smegmatis* mc<sup>2</sup>155 *groEL1ΔC* and at 32°C for 10-15 days  
347 for *M. marinum*.

348

### 349 **Construction of plasmids**

350 For construction of pSD26::*lipY* and pSD26::*lipYΔPE*, *M. tuberculosis* H37Rv genomic DNA was  
351 used as template as previously described [28]. The *lipY* gene was amplified by PCR using primers  
352 pSDlipY-F and pSDlipY-R and *lipYΔPE* was PCR-amplified using primers lipYΔPE-F and pSDlipY-  
353 R (**Table 1**). The corresponding amplicons harboring specific restrictions sites were digested with  
354 BamHI and cloned into pSD26 [77] under the control of the acetamidase inducible promoter and use  
355 to express and purify the recombinant proteins in *M. smegmatis*.

356 To construct pSD26::*lipYΔ149* and pSD26::*lipYΔ170*, the *lipYΔ149* and *lipYΔ170* genes were  
357 amplified from pSD26::*lipY* using the primers pSDlipYΔ149-F/pSDlipYΔPE-R and pSDlipYΔ170-  
358 F/pSDlipY-R respectively (**Table 1**). The pSD26::*lipY*<sup>G149D</sup> and pSD26::*lipY*<sup>E92A</sup> constructs were

359 generated by site directed mutagenesis using primers G149D-F/R and E92A-F/R primers,  
360 respectively (**Table 1**).

361 To generate pSD26::*PE-SGA-lipYΔ149* and pSD26::*PE-SGA-lipYΔ170*, a two-step cloning procedure  
362 was applied. Briefly, the PE domains for *PE-SGA-lipYΔ149* and *PE-SGA-lipYΔ170* genes were  
363 amplified from pSD26-*lipY* using primers pSDlipY-F/PE-149-R and pSDlipY-F/PE-170-R,  
364 respectively. In parallel, the *lipYΔ149* and *lipYΔ170* fragments were PCR-amplified from  
365 pSD26::*lipY* using primers PE-149-F/pSDlipY-R and PE-170-F/pSDlipY-R, respectively. The  
366 complete DNA fragments corresponding to *PE-SGA-lipYΔ149* and *PE-SGA-lipYΔ170* were obtained  
367 by overlapping PCR using primers pSDlipY-F and pSDlipY-R along with a mixture of the both DNA  
368 template (**Table 1**). The final PCR products were purified, digested with BamHI and cloned into  
369 BamHI-restricted pSD26, yielding pSD26::*PE-SGA-lipYΔ149* and the pSD26::*PE-SGA-lipYΔ170*.

370 To produce the constitutive expression vectors, *lipY*, *lipY<sup>E92A</sup>*, *lipY<sup>G149D</sup>*, *PE-SGA-lipYΔ149* and *PE-*  
371 *SGA-lipYΔ170* were PCR-amplified from their respective pSD26 derivatives using primers pVV-  
372 lipY-F/pVV-lipY-R. The *lipYΔ149* gene was amplified using pSD26::*lipYΔ149* as template and  
373 primers pVV-lipY-F/pVV-lipYΔ149-R. All DNA fragments were further digested with NdeI and  
374 HindIII restrictions enzymes (*Promega*, Charbonnieres, France) and subsequently cloned within  
375 pVV16 in frame with a C-terminal 6×Histidine coding sequence. The resulting plasmids were  
376 introduced in *E. coli* DH10B, analyzed by DNA sequencing (*GATC Biotech*, Germany) and used to  
377 transform *M. marinum*, as previously described [78].

378

### 379 **Expression and purification of recombinant proteins**

380 Expression and purification of recombinant proteins were performed as previously reported [45] with  
381 some modifications. Briefly, *M. smegmatis* mc<sup>2</sup>155 *groEL1ΔC* strain carrying pSD26-*lipY* or  
382 truncated forms of *lipY* or mutated *lipY*, were used to inoculate 20 mL of complete 7H9 Middlebrook  
383 medium containing 50 μg/mL hygromycin B during 3 days at 37°C under shaking (220 rpm). The  
384 preparation (OD<sub>600nm</sub> = 3.0-6.0) were used to inoculate 400 mL of culture medium (OD<sub>600nm</sub> = 0.1)

385 for a large-scale production. Bacteria were grown at 37°C with shaking (220 rpm) until an OD<sub>600nm</sub>  
386 value between 2.5 and 3.0 was reached and protein expression was induced by adding acetamide  
387 (*Sigma-Aldrich*, Saint-Quentin Fallavier, France) to a final concentration of 0.2% (w/v) for 16 h.  
388 Bacteria were harvested, re-suspended in ice-cold buffer A (30 mL 10 mM Tris/HCl pH 8.0, 150 mM  
389 NaCl) containing 1% *N*-lauroylsarcosine and were broken using a French Pressure cell at 1,100 psi.  
390 After centrifugation, the supernatant (S1) was recovered while the resulting pellet was re-suspended  
391 in buffer A (30 mL) and sonicated twice during 30 s with 30 s breaks between each cycle and stirred  
392 overnight at 4°C. After centrifugation, the new supernatant (S2) was pooled with S1 supernatant and  
393 both supernatants were loaded onto a Ni<sup>2+</sup>-NTA resin beforehand equilibrated with buffer A. The  
394 column was subsequently washed with buffer A without detergent prior to elution with increasing  
395 concentrations of imidazole. The eluted fractions were analyzed by performing on 12% SDS/PAGE  
396 as described by [79]. Fractions containing pure proteins were pooled, purified by size exclusion  
397 chromatography with a Hiload 16/60 Superdex 200 gel filtration column using buffer A; then  
398 concentrated by ultrafiltration to a final concentration of 0.6 mg/mL and stored at -80°C. Theoretical  
399 physical properties (molecular mass, extinction coefficient at 280 nm and isoelectric point) of all  
400 proteins containing the 6×His-tag were obtained from the ProtParam tool  
401 (<http://ca.expasy.org/tools/protparam.html>).

402

### 403 **Lipase activity**

404 Enzymatic hydrolysis of TAG emulsions, namely tributyrin (TC4), trioctanoin (TC8) or olive oil  
405 (TC18), were monitored titrimetrically for 10 min at 37°C using a pH-stat (Metrohm 718 STAT  
406 Titrino; *Metrohm Ltd.*, Switzerland). Assays were performed in 2.5 mM Tris-HCl buffer (pH 7.5)  
407 containing 300 mM NaCl and 3 mM NaTDC (Sodium taurodeoxycholate). Free fatty acids (FFA)  
408 released were automatically titrated with 0.1 N NaOH (0.01 N NaOH for titration the free fatty acids  
409 derived from olive oil) to maintain a fixed end-point pH value of 7.5. The specific activities of

410 enzymes were expressed in units per mg of pure enzyme. One unit corresponds to the release of one  
411  $\mu$ mole of fatty acid per minute.

412

### 413 **Generation of ILI-positive cells, lipid extraction and analysis**

414 *M. smegmatis* strains harboring plasmids pSD26, pSD26::*lipY*, pSD26::*lipY $\Delta$ PE*, pSD26::*lipY $\Delta$ 149*  
415 and pSD26::*lipY $\Delta$ 170* were grown in 7H9 Middlebrook complete medium containing 50  $\mu$ g/mL  
416 hygromycin B at 37°C under shaking 220 rpm until an OD<sub>600nm</sub> value between 1-1.5 was reached.  
417 After centrifugation for 10 min at 5,000 g, pellets were then washed with sterile Phosphate Buffer  
418 Saline (PBS) buffer pH 7.4 containing 0.05% Tween-20 (PBS-T), with classic sterile PBS buffer and  
419 finally normalized and re-suspend at OD<sub>600nm</sub> = 10 in sterile PBS. Subsequently, solution of PBS-  
420 containing bacteria was used to inoculate with an initial OD<sub>600nm</sub> of 0.05 a fresh Minimal Mineral Salt  
421 Medium Nitrogen Limiting (MSM NL) (Na<sub>2</sub>HPO<sub>4</sub> 2 g/L, KH<sub>2</sub>PO<sub>4</sub> 1 g/L, NaCl 0.5 g/L, MgSO<sub>4</sub> 0.2  
422 g/L and NH<sub>4</sub>Cl 0.05 g/L) containing 1 % glycerol as carbon source as previously described [53]. Cells  
423 were grown for 48 h at 37°C and 220 rpm in the presence of 50  $\mu$ g/mL hygromycin B and 0.02%  
424 (v/v) tyloxapol to avoid any clump formation. Induction of recombinant proteins was performed by  
425 adding 0.2% (w/v) acetamide. After 6 or 12 h of induction, the cells were collected by centrifugation  
426 during 15 min at 5,000 g.

427 Cells were washed three times in distilled water, lyophilized overnight and weighed to calculate the  
428 exact mass of mycobacterial dry extract. Apolar lipids were extracted as previously described [80].  
429 Briefly, 2 mL of MeOH-0.3% NaCl (10:1, v/v) were added per 50 mg dry extract. The saline-MeOH  
430 solution containing the bacterial dry extract was mixed with 1 mL of petroleum ether in Pyrex<sup>®</sup> tube  
431 and incubated at RT onto a tube rotator for at least 15 min. After centrifugation at 3,000 g during  
432 5 min, the upper organic layer was transferred to a fresh tube. This step was repeated three times and  
433 a final centrifugation was done for 15 min at 3,000 g to remove residues carried over during the  
434 extraction. The upper organic layer containing apolar lipids was transferred to a fresh pre-weighted  
435 vial, and the solvent was evaporated to dryness under a stream of nitrogen. The obtained apolar lipids

436 fraction containing TAG were then re-suspended in 300  $\mu$ L dichloromethane and analyzed by Thin  
437 layer chromatography (TLC) using aluminum TLC plates (Silica Gel 60, *Merck*) using  
438 heptane/diethyl ether/formic acid mixture (55:45:1 v/v/v) as eluent. The spots were visualized by  
439 vaporization of a saturated copper acetate-85% orthophosphoric acid (1:1, v/v) and charring. Plates  
440 were then scanned using a Chemidoc<sup>TM</sup> MP Imaging System (*Bio-Rad*) and densitometric analyses  
441 done using the ImageLab<sup>TM</sup> software version 5.0 (*Bio-Rad*) to determine relative TAG content in  
442 each sample.

443

#### 444 ***In silico* protein modelling**

445 All three-dimensional model structures were built with the automatic protein structure homology  
446 modeling server using the I-Tasser software program [81, 82]. LipY, LipY $\Delta$ PE were generated using  
447 the 4Q3O PDB code [83] as structural template and were already published in [14]. Regarding  
448 LipY $\Delta$ 149 and LipY $\Delta$ 170 their 3D-model structures were generated using the 4XVC PDB code [84]  
449 as template. The final model structures of LipY $\Delta$ 149 (93% coverage; normalized Z-score = 3.01; C-  
450 score=0.09) and LipY $\Delta$ 170 (97% coverage; normalized Z-score = 3.03; C-score=0.13) were  
451 visualized using the PyMOL Molecular Graphics System (version 1.4, Schrödinger, LLC).

452

#### 453 **Enzyme adsorption kinetics onto DOPG monomolecular films**

454 All experiments were performed at room temperature (RT) using home-made Teflon trough (volume,  
455 9.4 mL; surface area, 8.5 cm<sup>2</sup>) and the KSV5000 barostat equipment (*KSV Nima*, Helsinki, Finland)  
456 equipped with a Langmuir film balance to measure the surface pressure ( *$\Pi$* ), and monitored by the  
457 KSV Device Server Software v.3.50 as previously described [57, 85]. Before each experiment, the  
458 Teflon trough was cleaned with tap water, and then gently brushed in the presence of distilled ethanol,  
459 before being washed again with tap water and abundantly rinsed with Milli-Q water. The Teflon  
460 trough was filled with 10 mM Tris-HCl buffer (pH 7.5) containing 150 mM NaCl, prepared with  
461 Milli-Q water and filtered through a 0.45  $\mu$ m Millipore membrane. Residual surface-active impurities

462 were removed before each experiment by simultaneous sweeping and suction of the surface. The  
463 monolayer was prepared by spreading a few microliters of a DOPG solution (1 mg/mL in chloroform)  
464 over the clean air/buffer interface of the cylindrical trough using a high precision Hamilton  
465 microsyringe until the desired initial surface pressure ( $\Pi_i$ ) was reached. The waiting time for the  
466 spreading solvent evaporation and for the film to reach equilibrium vary from 10 to 20 min depending  
467 on the volume spread and the initial surface pressure. After solvent evaporation and stabilization of  
468 the film, the lipase was injected into the aqueous subphase at a final concentration of 40 nM and the  
469 surface pressure increase due to the adsorption/penetration of the lipase onto the DOPG  
470 monomolecular film was continuously recorded until the equilibrium surface pressure ( $\Pi_e$ ) was  
471 reached [56, 57]. At this stage, data recording was maintained to ensure that a plateau value in terms  
472 of surface pressure had been well reached. The aqueous sub-phase was continuously stirred with a 1-  
473 cm magnetic bar stirring at 250 rpm.

474

## 475 **Fourier Transform infrared (FTIR) spectroscopy**

### 476 *Sample preparation*

477 Multilamellar liposomes were obtained by hydrating 2% (w/v) DOPG powder with 100 mM  
478 phosphate buffer pH 8 containing 150 mM NaCl. Samples were vortexed extensively above and  
479 below the main phase transition temperature ( $T_m = -18^\circ\text{C}$ ), by using liquid nitrogen ( $\text{N}_2$ ). Three  
480 heating and cooling cycles were carried out. Protein lipid interaction was carried out by adding  
481 different protein sample concentrated to 1 mg/mL to the lipid mixture in order to reach a 1:10 (w/w)  
482 protein: lipid ratio. Control sample was made by adding the same volume of protein buffer to the lipid  
483 mixture.

484

### 485 *FTIR measurement*

486 IR spectra were recorded with a Jasco FT-IR 6100 equipped with a liquid  $\text{N}_2$  refrigerated Mercury-  
487 cadmium-telluride detector, the spectrometer was continuously purged with dried air. Spectra were  
488 collected using samples solution placed between two  $\text{CaF}_2$  windows separated with 5  $\mu\text{m}$

489 polyethylene terephthalate film spacers. Then, the FTIR cell was placed in a thermostated cell holder.  
490 Temperature was controlled with a pike technologies temperature controller working with the Peltier  
491 effect. The sample was equilibrated for 5 min at the required temperature before beginning the  
492 recording. The FTIR measurements were recorded between 4,000 and 800  $\text{cm}^{-1}$ . Each spectrum was  
493 obtained by averaging 88 scans recorded at a resolution of 0.5  $\text{cm}^{-1}$ . In order to determine the  
494 symmetric  $\nu_s(\text{CH}_2)$  and antisymmetric  $\nu_{as}(\text{CH}_2)$  methylene stretching wave numbers, a polynomial  
495 baseline was subtracted (Jasco spectra analysis software) in order to overcome the water stretching  
496 vibration contribution. All the data were obtained in duplicate from independent samples.

497

#### 498 **Extraction of surface-exposed proteins and immunoblotting**

499 Approximately 10 OD<sub>600</sub> unit of bacterial cultures were harvested for 10 min at 4,000 g and the pellet  
500 washed twice in PBS containing 0.05% Tween-20. Surface-exposed proteins were then isolated by  
501 incubating the bacteria with PBS containing 0.5% Genapol<sup>®</sup>-X080 (v/v) (*Sigma-Aldrich*, Saint-  
502 Quentin Fallavier, France) at RT, as previously reported [25]. Control samples were treated with a  
503 PBS buffer devoid of Genapol<sup>®</sup>-X080 detergent. After 30 min, supernatants were collected and  
504 precipitated with a final concentration of 12% trichloroacetic acid and proteins separated onto a 12%  
505 SDS-PAGE and transferred onto a nitrocellulose membrane using a Trans-Blot Turbo Transfer  
506 System (*Bio-Rad*). Immunoblotting of  $\delta$ His-tagged proteins was performed using a HisProbe<sup>™</sup> HRP  
507 conjugate (*Thermo-Scientific*). The exported MMAR\_0427 (which shares 89% of identity with the  
508 *M. tuberculosis* monoglyceride lipase Rv0183 protein found to be exported to the mycobacterial cell-  
509 wall and involved in mycobacterial cell-wall remodeling [46, 86]) was used as control for subcellular  
510 location. Immunoblotting was performed by cross reaction using rabbit polyclonal antibodies and  
511 horseradish peroxidase-conjugated anti-rabbit IgG (*Sigma Aldrich*). Detection was achieved using  
512 Pierce<sup>™</sup> ECL Western Blotting substrate solution (*Thermo-Scientific*) and visualized with a  
513 ChemiDoc<sup>™</sup> MP System (*Bio-Rad*).

514

515 **N-terminal sequencing of surface-exposed PE-SGA-LipY $\Delta$ 170**

516 *M. marinum* harboring pVV16::*PE-SGA-lipY $\Delta$ 170* was grown till the OD reaches 1-1.5 and collected  
517 by centrifugation 15 min 5,000 *g* at 4°C. The pellet was then washed twice with PBS and resuspended  
518 in PBS containing 0.5% Genapol<sup>®</sup>-X080 and stirred for 1 h at RT. The supernatant was recovered  
519 and precipitated with a final concentration of 12% trichloroacetic acid. Proteins were solubilized in  
520 10 mM Tris/HCl pH 8.0, 150 mM NaCl buffer containing 8M urea and subjected to Ni<sup>2+</sup>-NTA affinity  
521 chromatography. The eluted fractions were analyzed by 12% SDS/PAGE [79] and those containing  
522 pure proteins were pooled and transferred onto polyvinylidene fluoride (PVDF) membrane. The  
523 membrane was stained with Ponceau Red and the corresponding band was excised from the gel,  
524 washed 3 times in ethanol/water (90:10) solution, dried and subjected to N-terminal Edman  
525 sequencing using a Shimadzu PPSQ 31B protein sequencer.

526 **ACKNOWLEDGMENTS**

527 P. Santucci PhD fellowship was funded by the Ministère de l'Enseignement Supérieur, de la  
528 Recherche et de l'Innovation. N. Smichi post-doctoral fellowship was supported by a research grant  
529 from the University Hospital Institute "Méditerranée Infection". S. Diomande PhD fellowship was  
530 funded by Campus France (Paris, France). Financial support for this work was provided by the CNRS  
531 and Aix-Marseille Université. This work has benefited from the facilities and expertise of the  
532 proteomic platform of IMM FR3479 CNRS. All the authors would like to warmly thank Chantal de  
533 Chastellier for her involvement in the correction of this article, scientific discussions and her expertise  
534 in electron microscopy.

535

536 **AUTHOR'S CONTRIBUTIONS**

537 Conceived and design the experiments: PS, JFC, LK and SC

538 Performed the experiments: PS, NS, SD, IP, VP and HG

539 Analyzed the data: PS, NS, SD, VP, HG, JFC, LK and SC

540 Contributed reagents/materials/analysis tools: JFC, LK and SC

541 Wrote the manuscript: PS, HG, JFC, LK and SC with the help of CdC

542 All this work was supervised by SC

543

544 **ABBREVIATIONS**

545 Proline-Glutamic acid (PE); Fourier Transform infrared spectroscopy (FTIR); Tuberculosis (TB);

546 Latent Tuberculosis (LTBI); Intracellular Lipid Inclusion (ILI); Hormone-Sensitive Lipase (*h*HSL);

547 Triacylglycerol (TAG); Fatty acids (FFA); Specific Activity (SA); 1,2-dioleoyl-*sn*-glycero-3-

548 phosphoglycerol (DOPG); Polyvinylidene fluoride (PVDF); Luria Bertani (LB); Tributyrin (TC4);

549 Trioctanoin (TC8); Triolein (TC18); Room temperature (RT); Phosphate Buffered Saline (PBS);

550 Minimal Mineral Salt Medium Nitrogen Limiting (MSM NL); Thin layer chromatography (TLC).

551

552 **CONFLICTS OF INTEREST**

553 The authors have no conflict of interest to declare.

554 **REFERENCES**

- 555 1. WHO (2018) Global Tuberculosis Report.
- 556 2. Dutta, N. K. & Karakousis, P. C. (2014) Latent tuberculosis infection: myths, models, and  
557 molecular mechanisms, *Microbiol Mol Biol Rev.* **78**, 343-71.
- 558 3. Getahun, H., Matteelli, A., Chaisson, R. E. & Raviglione, M. (2015) Latent Mycobacterium  
559 tuberculosis infection, *N Engl J Med.* **372**, 2127-35.
- 560 4. Esmail, H., Barry, C. E., 3rd, Young, D. B. & Wilkinson, R. J. (2014) The ongoing challenge of  
561 latent tuberculosis, *Philos Trans R Soc Lond B Biol Sci.* **369**, 20130437.
- 562 5. Bloch, H. & Segal, W. (1956) Biochemical differentiation of Mycobacterium tuberculosis grown  
563 in vivo and in vitro, *J Bacteriol.* **72**, 132-41.
- 564 6. McKinney, J. D., Honer zu Bentrup, K., Munoz-Elias, E. J., Miczak, A., Chen, B., Chan, W. T.,  
565 Swenson, D., Sacchetti, J. C., Jacobs, W. R., Jr. & Russell, D. G. (2000) Persistence of  
566 Mycobacterium tuberculosis in macrophages and mice requires the glyoxylate shunt enzyme  
567 isocitrate lyase, *Nature.* **406**, 735-8.
- 568 7. Munoz-Elias, E. J. & McKinney, J. D. (2005) Mycobacterium tuberculosis isocitrate lyases 1 and  
569 2 are jointly required for in vivo growth and virulence, *Nat Med.* **11**, 638-44.
- 570 8. Garton, N. J., Waddell, S. J., Sherratt, A. L., Lee, S. M., Smith, R. J., Senner, C., Hinds, J.,  
571 Rajakumar, K., Adegbola, R. A., Besra, G. S., Butcher, P. D. & Barer, M. R. (2008) Cytological and  
572 transcript analyses reveal fat and lazy persister-like bacilli in tuberculous sputum, *PLoS Med.* **5**, e75.
- 573 9. Guirado, E., Mbawuike, U., Keiser, T. L., Arcos, J., Azad, A. K., Wang, S. H. & Schlesinger, L.  
574 S. (2015) Characterization of host and microbial determinants in individuals with latent tuberculosis  
575 infection using a human granuloma model, *MBio.* **6**, e02537-14.
- 576 10. Peyron, P., Vaubourgeix, J., Poquet, Y., Levillain, F., Botanch, C., Bardou, F., Daffe, M., Emile,  
577 J. F., Marchou, B., Cardona, P. J., de Chastellier, C. & Altare, F. (2008) Foamy macrophages from  
578 tuberculous patients' granulomas constitute a nutrient-rich reservoir for M. tuberculosis persistence,  
579 *PLoS Pathog.* **4**, e1000204.

- 580 11. Daniel, J., Maamar, H., Deb, C., Sirakova, T. D. & Kolattukudy, P. E. (2011) *Mycobacterium*  
581 *tuberculosis* uses host triacylglycerol to accumulate lipid droplets and acquires a dormancy-like  
582 phenotype in lipid-loaded macrophages, *PLoS Pathog.* **7**, e1002093.
- 583 12. Podinovskaia, M., Lee, W., Caldwell, S. & Russell, D. G. (2013) Infection of macrophages with  
584 *Mycobacterium tuberculosis* induces global modifications to phagosomal function, *Cell Microbiol.*  
585 **15**, 843-59.
- 586 13. Caire-Brandli, I., Papadopoulos, A., Malaga, W., Marais, D., Canaan, S., Thilo, L. & de  
587 Chastellier, C. (2014) Reversible Lipid Accumulation and Associated Division Arrest of  
588 *Mycobacterium avium* in Lipoprotein-Induced Foamy Macrophages May Resemble Key Events  
589 during Latency and Reactivation of Tuberculosis, *Infect Immun.* **82**, 476-90.
- 590 14. Santucci, P., Diomande, S., Poncin, I., Alibaud, L., Viljoen, A., Kremer, L., de Chastellier, C. &  
591 Canaan, S. (2018) Delineating the physiological roles of the PE and catalytic domain of LipY in lipid  
592 consumption in mycobacteria-infected foamy macrophages, *Infect Immun.* **86**, e00394-18.
- 593 15. Low, K. L., Rao, P. S., Shui, G., Bendt, A. K., Pethe, K., Dick, T. & Wenk, M. R. (2009)  
594 Triacylglycerol utilization is required for regrowth of in vitro hypoxic nonreplicating *Mycobacterium*  
595 *bovis* bacillus Calmette-Guerin, *J Bacteriol.* **191**, 5037-43.
- 596 16. Santucci, P., Bouzid, F., Smichi, N., Poncin, I., Kremer, L., De Chastellier, C., Drancourt, M. &  
597 Canaan, S. (2016) Experimental Models of Foamy Macrophages and Approaches for Dissecting the  
598 Mechanisms of Lipid Accumulation and Consumption during Dormancy and Reactivation of  
599 Tuberculosis, *Front Cell Infect Microbiol.* **6**, 122.
- 600 17. Cole, S. T., Brosch, R., Parkhill, J., Garnier, T., Churcher, C., Harris, D., Gordon, S. V.,  
601 Eiglmeier, K., Gas, S., Barry, C. E., 3rd, Tekaia, F., Badcock, K., Basham, D., Brown, D.,  
602 Chillingworth, T., Connor, R., Davies, R., Devlin, K., Feltwell, T., Gentles, S., Hamlin, N., Holroyd,  
603 S., Hornsby, T., Jagels, K., Barrell, B. G. & et al. (1998) Deciphering the biology of *Mycobacterium*  
604 *tuberculosis* from the complete genome sequence, *Nature.* **393**, 537-44.

- 605 18. Camus, J., Pryor, M., Medigue, C. & Cole, S. (2002) Re-annotation of the genome sequence of  
606 *Mycobacterium tuberculosis* H37Rv, *Microbiology*. **148**, 2967-73.
- 607 19. Tekaiia, F., Gordon, S. V., Garnier, T., Brosch, R., Barrell, B. G. & Cole, S. T. (1999) Analysis  
608 of the proteome of *Mycobacterium tuberculosis* in silico, *Tuber Lung Dis*. **79**, 329-42.
- 609 20. Mukhopadhyay, S. & Balaji, K. N. (2011) The PE and PPE proteins of *Mycobacterium*  
610 *tuberculosis*, *Tuberculosis (Edinb)*. **91**, 441-7.
- 611 21. Brennan, M. J. (2017) The Enigmatic PE/PPE Multigene Family of *Mycobacteria* and  
612 *Tuberculosis* Vaccination, *Infect Immun*. **85**.
- 613 22. Basu, S., Pathak, S. K., Banerjee, A., Pathak, S., Bhattacharyya, A., Yang, Z., Talarico, S.,  
614 Kundu, M. & Basu, J. (2007) Execution of macrophage apoptosis by PE\_PGRS33 of *Mycobacterium*  
615 *tuberculosis* is mediated by Toll-like receptor 2-dependent release of tumor necrosis factor-alpha, *J*  
616 *Biol Chem*. **282**, 1039-50.
- 617 23. Brennan, M. J., Delogu, G., Chen, Y., Bardarov, S., Kriakov, J., Alavi, M. & Jacobs, W. R., Jr.  
618 (2001) Evidence that mycobacterial PE\_PGRS proteins are cell surface constituents that influence  
619 interactions with other cells, *Infect Immun*. **69**, 7326-33.
- 620 24. Abdallah, A. M., Verboom, T., Weerdenburg, E. M., Gey van Pittius, N. C., Mahasha, P. W.,  
621 Jimenez, C., Parra, M., Cadieux, N., Brennan, M. J., Appelmelk, B. J. & Bitter, W. (2009) PPE and  
622 PE\_PGRS proteins of *Mycobacterium marinum* are transported via the type VII secretion system  
623 ESX-5, *Mol Microbiol*. **73**, 329-40.
- 624 25. Daleke, M. H., Cascioferro, A., de Punder, K., Ummels, R., Abdallah, A. M., van der Wel, N.,  
625 Peters, P. J., Luirink, J., Manganelli, R. & Bitter, W. (2011) Conserved Pro-Glu (PE) and Pro-Pro-  
626 Glu (PPE) protein domains target LipY lipases of pathogenic mycobacteria to the cell surface via the  
627 ESX-5 pathway, *J Biol Chem*. **286**, 19024-34.
- 628 26. Daleke, M. H., Ummels, R., Bawono, P., Heringa, J., Vandenbroucke-Grauls, C. M., Luirink, J.  
629 & Bitter, W. (2012) General secretion signal for the mycobacterial type VII secretion pathway,  
630 *Proceedings of the National Academy of Sciences of the United States of America*. **109**, 11342-7.

- 631 27. Cascioferro, A., Daleke, M. H., Ventura, M., Dona, V., Delogu, G., Palu, G., Bitter, W. &  
632 Manganelli, R. (2011) Functional dissection of the PE domain responsible for translocation of  
633 PE\_PGRS33 across the mycobacterial cell wall, *PLoS ONE*. **6**, e27713.
- 634 28. Mishra, K. C., de Chastellier, C., Narayana, Y., Bifani, P., Brown, A. K., Besra, G. S., Katoch,  
635 V. M., Joshi, B., Balaji, K. N. & Kremer, L. (2008) Functional role of the PE domain and  
636 immunogenicity of the *Mycobacterium tuberculosis* triacylglycerol hydrolase LipY, *Infect Immun*.  
637 **76**, 127-40.
- 638 29. Deb, C., Daniel, J., Sirakova, T. D., Abomoelak, B., Dubey, V. S. & Kolattukudy, P. E. (2006)  
639 A novel lipase belonging to the hormone-sensitive lipase family induced under starvation to utilize  
640 stored triacylglycerol in *Mycobacterium tuberculosis*, *J Biol Chem*. **281**, 3866-75.
- 641 30. Delorme, V., Diomande, S. V., Dedieu, L., Cavalier, J. F., Carriere, F., Kremer, L., Leclaire, J.,  
642 Fotiadu, F. & Canaan, S. (2012) MmPPOX inhibits *Mycobacterium tuberculosis* lipolytic enzymes  
643 belonging to the hormone-sensitive lipase family and alters mycobacterial growth, *PLoS ONE*. **7**,  
644 e46493.
- 645 31. Kapoor, N., Pawar, S., Sirakova, T. D., Deb, C., Warren, W. L. & Kolattukudy, P. E. (2013)  
646 Human granuloma in vitro model, for TB dormancy and resuscitation, *PLoS ONE*. **8**, e53657.
- 647 32. Brockman, H. (1999) Lipid monolayers: why use half a membrane to characterize protein-  
648 membrane interactions?, *Curr Opin Struct Biol*. **9**, 438-443.
- 649 33. de La Fournière, L., Ivanova, M. G., Blond, J.-P., Carrière, F. & Verger, R. (1994) Surface  
650 behaviour of human pancreatic and gastric lipases, *Colloids Surf B: Biointerfaces*. **2**, 585-593.
- 651 34. Boisselier, É., Calvez, P., Demers, É., Cantin, L. & Salesse, C. (2012) Influence of the physical  
652 state of phospholipid monolayers on protein binding, *Langmuir*. **28**, 9680-9688.
- 653 35. Bénarouche, A., Point, V., Parsiegla, G., Carrière, F. & Cavalier, J.-F. (2013) New insights into  
654 the pH-dependent interfacial adsorption of dog gastric lipase using the monolayer technique, *Colloids*  
655 *Surf B: Biointerfaces*. **111**, 306-312.

- 656 36. Bénarouche, A., Point, V., Carrière, F. & Cavalier, J.-F. (2014) An interfacial and comparative  
657 *in vitro* study of gastrointestinal lipases and *Yarrowia lipolytica* LIP2 lipase, a candidate for enzyme  
658 replacement therapy, *Biochimie*. **102**, 145-153.
- 659 37. Nitenberg, M., Bénarouche, A., Maniti, O., Marion, E., Marsollier, L., Géan, J., Dufourc, E. J.,  
660 Cavalier, J.-F., Canaan, S. & Girard-Egrot, A. P. (2018) The potent effect of mycolactone on lipid  
661 membranes, *PLoS Pathog.* **14**, e1006814.
- 662 38. Mendelsohn, R. & Moore, D. J. (1998) Vibrational spectroscopic studies of lipid domains in  
663 biomembranes and model systems, *Chem Phys Lipids*. **96**, 141-57.
- 664 39. Lewis, R. N. & McElhaney, R. N. (2013) Membrane lipid phase transitions and phase  
665 organization studied by Fourier transform infrared spectroscopy, *Biochim Biophys Acta*. **1828**, 2347-  
666 58.
- 667 40. Mateos-Diaz, E., Bakala N'Goma, J. C., Byrne, D., Robert, S., Carriere, F. & Gaussier, H. (2018)  
668 IR spectroscopy analysis of pancreatic lipase-related protein 2 interaction with phospholipids: 1.  
669 Discriminative recognition of mixed micelles versus liposomes, *Chem Phys Lipids*. **211**, 52-65.
- 670 41. Brennan, P. J. & Nikaido, H. (1995) The envelope of mycobacteria, *Annu Rev Biochem*. **64**, 29-  
671 63.
- 672 42. Minnikin, D. E., Lee, O. Y., Wu, H. H. T., Nataraj, V., Donoghue, H. D., Ridell, M., Watanabe,  
673 M., Alderwick, L., Bhatt, A. & Besra, G. S. (2015) Pathophysiological implications of cell envelope  
674 structure in *Mycobacterium tuberculosis* and related taxa in *Tuberculosis - Expanding Knowledge*  
675 (Ribón, W., ed) pp. 145-175, InTech Open Access Publisher.
- 676 43. Santucci, P., Point, V., Poncin, I., Guy, A., Crauste, C., Serveau-Avesque, C., Galano, J. M.,  
677 Spilling, C. D., Cavalier, J. F. & Canaan, S. (2018) LipG a bifunctional phospholipase/thioesterase  
678 involved in mycobacterial envelope remodeling, *Bioscience reports*. **38**, BSR20181953.
- 679 44. Noens, E. E., Williams, C., Anandhakrishnan, M., Poulsen, C., Ehebauer, M. T. & Wilmanns,  
680 M. (2011) Improved mycobacterial protein production using a *Mycobacterium smegmatis*  
681 groEL1DeltaC expression strain, *BMC Biotechnol.* **11**, 27.

- 682 45. Brust, B., Lecoufle, M., Tuailon, E., Dedieu, L., Canaan, S., Valverde, V. & Kremer, L. (2011)  
683 *Mycobacterium tuberculosis* lipolytic enzymes as potential biomarkers for the diagnosis of active  
684 tuberculosis, *PLoS ONE*. **6**, e25078.
- 685 46. Dhouib, R., Laval, F., Carriere, F., Daffe, M. & Canaan, S. (2010) A monoacylglycerol lipase  
686 from *Mycobacterium smegmatis* Involved in bacterial cell interaction, *J Bacteriol.* **192**, 4776-85.
- 687 47. Point, V., Malla, R. K., Diomande, S., Martin, B. P., Delorme, V., Carriere, F., Canaan, S., Rath,  
688 N. P., Spilling, C. D. & Cavalier, J. F. (2012) Synthesis and kinetic evaluation of cyclophostin and  
689 cyclipostins phosphonate analogs as selective and potent inhibitors of microbial lipases, *J Med Chem.*  
690 **55**, 10204-19.
- 691 48. Alvarez, H. M. & Steinbuchel, A. (2002) Triacylglycerols in prokaryotic microorganisms, *Appl*  
692 *Microbiol Biotechnol.* **60**, 367-76.
- 693 49. Garton, N., Christensen, H., Minnikin, D., Adegbola, R. & Barer, M. (2002) Intracellular  
694 lipophilic inclusions of mycobacteria in vitro and in sputum., *Microbiology.* **148**, 2951-8.
- 695 50. Kremer, L., de Chastellier, C., Dobson, G., Gibson, K. J., Bifani, P., Balor, S., Gorvel, J. P.,  
696 Locht, C., Minnikin, D. E. & Besra, G. S. (2005) Identification and structural characterization of an  
697 unusual mycobacterial monomeromycolyl-diacylglycerol, *Mol Microbiol.* **57**, 1113-26.
- 698 51. Sirakova, T. D., Dubey, V. S., Deb, C., Daniel, J., Korotkova, T. A., Abomoelak, B. &  
699 Kolattukudy, P. E. (2006) Identification of a diacylglycerol acyltransferase gene involved in  
700 accumulation of triacylglycerol in *Mycobacterium tuberculosis* under stress, *Microbiology.* **152**,  
701 2717-25.
- 702 52. Viljoen, A., Blaise, M., de Chastellier, C. & Kremer, L. (2016) MAB\_3551c encodes the primary  
703 triacylglycerol synthase involved in lipid accumulation in *Mycobacterium abscessus*, *Mol Microbiol.*  
704 **102**, 611-627.
- 705 53. Santucci, J., Point, Poncin, Viljoen, Cavalier, Kremer, Canaan (2018) Nitrogen deprivation  
706 induces triacylglycerol accumulation, drug tolerance and hypervirulence in mycobacteria *Scientific*  
707 *reports*. **Submitted**.

708 54. Saxena, A. K., Roy, K. K., Singh, S., Vishnoi, S. P., Kumar, A., Kashyap, V. K., Kremer, L.,  
709 Srivastava, R. & Srivastava, B. S. (2013) Identification and characterisation of small-molecule  
710 inhibitors of Rv3097c-encoded lipase (LipY) of Mycobacterium tuberculosis that selectively inhibit  
711 growth of bacilli in hypoxia, *Int J Antimicrob Agents*. **42**, 27-35.

712 55. Garrett, C. K., Broadwell, L. J., Hayne, C. K. & Neher, S. B. (2015) Modulation of the Activity  
713 of Mycobacterium tuberculosis LipY by Its PE Domain, *PLoS ONE*. **10**, e0135447.

714 56. de la Fournière, L., Ivanova, M. G., Blond, J.-P., Carrière, F. & Verger, R. (1994) Surface  
715 behaviour of human pancreatic and gastric lipases, *Colloids and Surfaces*. **B2**, 585-593.

716 57. Benarouche, A., Point, V., Parsiegla, G., Carriere, F. & Cavalier, J. F. (2013) New insights into  
717 the pH-dependent interfacial adsorption of dog gastric lipase using the monolayer technique, *Colloids*  
718 *Surf B: Biointerfaces*. **111**, 306-12.

719 58. Boisselier, E., Calvez, P., Demers, E., Cantin, L. & Salesse, C. (2012) Influence of the physical  
720 state of phospholipid monolayers on protein binding, *Langmuir*. **28**, 9680-8.

721 59. Calvez, P., Bussieres, S., Eric, D. & Salesse, C. (2009) Parameters modulating the maximum  
722 insertion pressure of proteins and peptides in lipid monolayers, *Biochimie*. **91**, 718-33.

723 60. Calvez, P., Demers, E., Boisselier, E. & Salesse, C. (2011) Analysis of the contribution of  
724 saturated and polyunsaturated phospholipid monolayers to the binding of proteins, *Langmuir*. **27**,  
725 1373-9.

726 61. Kodati, V. R. & Lafleur, M. (1993) Comparison between orientational and conformational orders  
727 in fluid lipid bilayers, *Biophysical Journal*. **64**, 163-70.

728 62. Lewis, R. N., Pohle, W. & McElhaney, R. N. (1996) The interfacial structure of phospholipid  
729 bilayers: differential scanning calorimetry and Fourier transform infrared spectroscopic studies of  
730 1,2-dipalmitoyl-sn-glycero-3-phosphorylcholine and its dialkyl and acyl-alkyl analogs, *Biophysical*  
731 *Journal*. **70**, 2736-46.

- 732 63. Gaussier, H., Lavoie, M. & Subirade, M. (2003) Conformational changes of pediocin in an  
733 aqueous medium monitored by fourier transform infrared spectroscopy: a biological implication, *Int*  
734 *J Biol Macromol.* **32**, 1-9.
- 735 64. Lefevre, T. & Subirade, M. (2000) Interaction of beta-lactoglobulin with phospholipid bilayers:  
736 a molecular level elucidation as revealed by infrared spectroscopy, *Int J Biol Macromol.* **28**, 59-67.
- 737 65. Paolorossi, M. & Montich, G. G. (2011) Conformational changes of beta2-human glycoprotein I  
738 and lipid order in lipid-protein complexes, *Biochim Biophys Acta.* **1808**, 2167-77.
- 739 66. Cameron, D. G., Casal, H. L. & Mantsch, H. H. (1980) Characterization of the pretransition in  
740 1,2-dipalmitoyl-sn-glycero-3-phosphocholine by Fourier transform infrared spectroscopy,  
741 *Biochemistry.* **19**, 3665-72.
- 742 67. Cameron, D. G., Casal, H. L., Mantsch, H. H., Boulanger, Y. & Smith, I. C. (1981) The  
743 thermotropic behavior of dipalmitoyl phosphatidylcholine bilayers. A Fourier transform infrared  
744 study of specifically labeled lipids, *Biophys J.* **35**, 1-16.
- 745 68. Casal, H. L. & McElhaney, R. N. (1990) Quantitative determination of hydrocarbon chain  
746 conformational order in bilayers of saturated phosphatidylcholines of various chain lengths by Fourier  
747 transform infrared spectroscopy, *Biochemistry.* **29**, 5423-7.
- 748 69. Findlay, E. J. & Barton, P. G. (1978) Phase behavior of synthetic phosphatidylglycerols and  
749 binary mixtures with phosphatidylcholines in the presence and absence of calcium ions, *Biochemistry.*  
750 **17**, 2400-5.
- 751 70. Hinton, D. P. & Johnson, C. S. (1995) Diffusion Coefficients, Electrophoretic Mobilities, and  
752 Morphologies of Charged Phospholipid Vesicles by Pulsed Field Gradient NMR and Electron  
753 Microscopy, *J Colloid Interface Sci.* **173**, 364-371.
- 754 71. Mendelsohn, R., Dluhy, R. A., Crawford, T. & Mantsch, H. H. (1984) Interaction of glycophorin  
755 with phosphatidylserine: a Fourier transform infrared investigation, *Biochemistry.* **23**, 1498-504.
- 756 72. Mendelsohn, R., Brauner, J. W., Faines, L., Mantsch, H. H. & Dluhy, R. A. (1984) Calorimetric  
757 and Fourier transform infrared spectroscopic studies on the interaction of glycophorin with

758 phosphatidylserine/dipalmitoylphosphatidylcholine-d62 mixtures, *Biochim Biophys Acta.* **774**, 237-  
759 46.

760 73. Heinz, C. & Niederweis, M. (2000) Selective extraction and purification of a mycobacterial outer  
761 membrane protein, *Anal Biochem.* **285**, 113-20.

762 74. Sani, M., Houben, E. N., Geurtsen, J., Pierson, J., de Punder, K., van Zon, M., Wever, B., Piersma,  
763 S. R., Jimenez, C. R., Daffe, M., Appelmelk, B. J., Bitter, W., van der Wel, N. & Peters, P. J. (2010)  
764 Direct visualization by cryo-EM of the mycobacterial capsular layer: a labile structure containing  
765 ESX-1-secreted proteins, *PLoS Pathog.* **6**, e1000794.

766 75. van der Woude, A. D., Mahendran, K. R., Ummels, R., Piersma, S. R., Pham, T. V., Jimenez, C.  
767 R., de Punder, K., van der Wel, N. N., Winterhalter, M., Luirink, J., Bitter, W. & Houben, E. N.  
768 (2013) Differential detergent extraction of mycobacterium marinum cell envelope proteins identifies  
769 an extensively modified threonine-rich outer membrane protein with channel activity, *J Bacteriol.*  
770 **195**, 2050-9.

771 76. Stinear, T. P., Seemann, T., Harrison, P. F., Jenkin, G. A., Davies, J. K., Johnson, P. D., Abdellah,  
772 Z., Arrowsmith, C., Chillingworth, T., Churcher, C., Clarke, K., Cronin, A., Davis, P., Goodhead, I.,  
773 Holroyd, N., Jagels, K., Lord, A., Moule, S., Mungall, K., Norbertczak, H., Quail, M. A.,  
774 Rabbinowitsch, E., Walker, D., White, B., Whitehead, S., Small, P. L., Brosch, R., Ramakrishnan,  
775 L., Fischbach, M. A., Parkhill, J. & Cole, S. T. (2008) Insights from the complete genome sequence  
776 of Mycobacterium marinum on the evolution of Mycobacterium tuberculosis, *Genome Res.* **18**, 729-  
777 41.

778 77. Daugelat, S., Kowall, J., Mattow, J., Bumann, D., Winter, R., Hurwitz, R. & Kaufmann, S. H.  
779 (2003) The RD1 proteins of Mycobacterium tuberculosis: expression in Mycobacterium smegmatis  
780 and biochemical characterization, *Microbes Infect.* **5**, 1082-95.

781 78. Goude, R., Roberts, D. M. & Parish, T. (2015) Electroporation of mycobacteria, *Methods Mol*  
782 *Biol.* **1285**, 117-30.

783 79. Laemmli, U. K. (1970) Cleavage of structural proteins during the assembly of the head of  
784 bacteriophage T4, *Nature*. **227**, 680-685.

785 80. Besra, G. S. (1998) Preparation of cell-wall fractions from mycobacteria, *Methods Mol Biol*. **101**,  
786 91-107.

787 81. Roy, A., Kucukural, A. & Zhang, Y. (2010) I-TASSER: a unified platform for automated protein  
788 structure and function prediction, *Nature Protocols*. **5**, 725-38.

789 82. Zhang, Y. (2008) I-TASSER server for protein 3D structure prediction, *BMC bioinformatics*. **9**,  
790 40.

791 83. Alcaide, M., Stogios, P. J., Lafraya, A., Tchigvintsev, A., Flick, R., Bargiela, R., Chernikova, T.  
792 N., Reva, O. N., Hai, T., Leggewie, C. C., Katzke, N., La Cono, V., Matesanz, R., Jebbar, M., Jaeger,  
793 K. E., Yakimov, M. M., Yakunin, A. F., Golyshin, P. N., Golyshina, O. V., Savchenko, A. & Ferrer,  
794 M. (2015) Pressure adaptation is linked to thermal adaptation in salt-saturated marine habitats,  
795 *Environ Microbiol*. **17**, 332-45.

796 84. Li, P.-Y., Chen, X.-L., Ji, P., Li, C.-Y., Wang, P., Zhang, Y., Xie, B.-B., Qin, Q.-L., Su, H.-N.,  
797 Zhou, B.-C., Zhang, Y.-Z. & Zhang, X.-Y. (2015) Interdomain Hydrophobic Interactions Modulate  
798 the Thermostability of Microbial Esterases from the Hormone-Sensitive Lipase Family, *J Biol Chem*.  
799 **290**, 11188-11198.

800 85. Benarouche, A., Sams, L., Bourlieu, C., Vie, V., Point, V., Cavalier, J. F. & Carriere, F. (2017)  
801 Studying Gastric Lipase Adsorption Onto Phospholipid Monolayers by Surface Tensiometry,  
802 Ellipsometry, and Atomic Force Microscopy, *Methods Enzymol*. **583**, 255-278.

803 86. Cotes, K., Dhouib, R., Douchet, I., Chahinian, H., de Caro, A., Carriere, F. & Canaan, S. (2007)  
804 Characterization of an exported monoglyceride lipase from *Mycobacterium tuberculosis* possibly  
805 involved in the metabolism of host cell membrane lipids, *Biochem J*. **408**, 417-27.

806

807

## 808 TABLES

809 **Table 1. Primers used in this study.** Nucleotides of the primers that differ from the wild-type  
 810 sequence are presented in bold and restriction sites incorporated into the primers are underlined and  
 811 their name is indicated in parenthesis.

Primers	Sequence 5' → 3'	Origin
pSDlipY-F	AA <u><b>GGATCC</b></u> GTGTCTTATGTTGTTGCGTTG ( <b>BamHI</b> )	[28]
pSDlipY-R	A <u><b>GGATCC</b></u> GGCGATACCGAGTTGCTG ( <b>BamHI</b> )	[28]
pSDlipYΔPE-F	AA <u><b>GGATCC</b></u> TCGCCAGCGGTATCGGGAACGG ( <b>BamHI</b> )	[28]
pSDlipYΔPE-R	A <u><b>GGATCC</b></u> GGCGATACCGAGTTGCTG ( <b>BamHI</b> )	[28]
pSDlipYΔ149-F	AA <u><b>GGATCC</b></u> GCTGCCGATTTCGACATCGC ( <b>BamHI</b> )	This study
pSDlipYΔ170-F	AA <u><b>GGATCC</b></u> GAAACTCACTTTGCAATCCCAAACAATCCAC ( <b>BamHI</b> )	This study
E92A-F	GCCGCCCGCGCTGGCCAAC	This study
E92A-R	GTTGGCCAGCGCGGCGGCGGC	This study
G149D-F	CTTCACCGGCACGCCGTCAGATGCTGCCGGATTTCGACATCGC	This study
G149D-R	GCGATGTCGATCCGGCAGCATCTGACGGCGTGCCGGTGAAG	This study
PE-149-F	CTGGCCAATGCTAGTGGGGCTGCCGGATTTCGAC	This study
PE-149-R	GTCGAATCCGGCAGCCCCACTAGCATTGGCCAG	This study
PE-170-F	CTGGCCAATGCTAGTGGGGCTGAAACTCACTTTGC	This study
PE-170-R	GCAAAGTGAGTTTCAGCCCCACTAGCATTGGCCAG	This study
pVV-lipY-F	GGAATCACTTCG <u><b>CATATG</b></u> GTTGTCTTATGTTGTTGCGTTGCG ( <b>NdeI</b> )	This study
pVV-lipY-R	GTGGTGGTGGTGA <u><b>AGCTT</b></u> GGCGGCGATCCGAGTTGCTG ( <b>HindIII</b> )	This study
pVV-lipYΔ149-F	GGAATCACTTCG <u><b>CATATG</b></u> GCTGCCGATTTCGACATCGC ( <b>NdeI</b> )	This study

812

813

814 **Table 2. Binding parameters ( $\Pi_c$ , synergy and  $\Delta\Pi_0$ ) of LipY, LipY $\Delta$ 149, LipY $\Delta$ 170 and**  
 815 **LipY $\Delta$ PE in the presence of a DOPG Monolayer <sup>a</sup>**

816

	LipY	LipY $\Delta$ 149	LipY $\Delta$ 170	LipY $\Delta$ PE
$\Pi_c$ (mN.m <sup>-1</sup> )	22.5 ± 1.2	16.4 ± 0.49	14.3 ± 0.25	17.2 ± 0.83
synergy	+0.113 ± 0.010	-0.023 ± 0.001	-0.177 ± 0.0045	-0.564 ± 0.043
$\Delta\Pi_0$ (mN.m <sup>-1</sup> )	20.0 ± 1.1	16.8 ± 0.50	16.9 ± 0.30	26.9 ± 1.3

817

818

819

820

821

822

823

824

<sup>a</sup> Data derived from **Figure 3A**. Experiments were carried out at 25°C in a cylindrical Teflon trough as described in **Experimental Procedures**. Buffer: 10 mM Tris-HCl (pH 7.5) containing 150 mM NaCl. Final enzyme concentration, 40 nM. Data are mean values of three independent assays. The uncertainty was calculated as previously described [59, 60].

825 **FIGURE LEGENDS**

826 **Figure 1: Biochemical characterization of LipY protein and its truncated forms.** A) Schematic  
827 representation of LipY and its mutant forms. The PE domain is highlighted in blue, the linker region  
828 before the Gly<sup>149</sup> maturation site is colored in green, the remaining linker region is colored in orange  
829 and the lipase domain is highlighted in grey. B) Protein purity assessed onto 12% SDS-PAGE, lane  
830 1 corresponds to the Unstained Protein Molecular Weight Marker (MW) (Euromedex), lanes 2 to 5  
831 correspond to 6 µg of LipY, LipYΔPE, LipYΔ149 and LipYΔ170, respectively, loaded onto the gel  
832 and stained with Coomassie blue. C-D-E). SA determination of LipY and its mutant forms using TC4  
833 (C), TC8 (D) and TC18 (E) as substrates. Experiments were carried out at 37°C in 15 mL of 2.5 mM  
834 Tris-HCl buffer (pH 7.5) containing 300 mM NaCl and 1 or 3 mM NaTDC for TC4 and TC8,  
835 respectively. Olive oil (TC18) was assayed in the same conditions without NaTDC and with 10%  
836 arabic gum. One international enzymatic unit corresponds to 1 µmole of fatty acid released per min.  
837 Values are means of 3 independent experiments ± S.D. F) Representation of the relative activities of  
838 the LipY truncated forms using TC4, TC8 and TC18 as substrates in comparison to the full-length  
839 LipY. \*\*, *p*-value < 0.01. \*, *p*-value < 0.05. Statistical analysis was done using one-way ANOVA  
840 followed by a post hoc Tukey's Honest Significant Difference test.

841

842 **Figure 2: Overexpression of *lipY* and its mutant forms within lipid-rich mycobacteria.** A)  
843 *M. smegmatis* recombinant strains harboring empty pSD26, pSD26::*lipY*, pSD26::*lipY*ΔPE,  
844 pSD26::*lipY*Δ149 and pSD26::*lipY*Δ170 were grown in minimal salt medium containing 0.05 g/L of  
845 NH<sub>4</sub>Cl and 1% glycerol as carbon source for 48 h to promote ILI formation. Bacteria were re-  
846 suspended in medium devoid of carbon, containing 0.2% (w/v) acetamide and were collected after  
847 6 h or 12 h of induction. Cells were lyophilized and the same amount of dry cell weight was used for  
848 apolar lipid extraction. TAG levels from each culture were analyzed by TLC with triolein as standard.  
849 The TLC plate is representative of individual experiments performed in duplicate. TLC densitometric  
850 analysis of relative TAG levels in each sample was performed by using the empty vector culture at

851 6h post-induction as a reference. Results are expressed as mean values  $\pm$  SD of two distinct and  
852 independent experiments. **B-E)** Three dimensional structure modeling of LipY protein and its  
853 truncated forms. The PE domain is highlighted in blue and the catalytic triad composed of serine  
854 (Ser<sup>309</sup>), aspartic acid (Asp<sup>383</sup>) and histidine (His<sup>414</sup>) residues are shown in yellow. The green part  
855 represents the polypeptide linking the catalytic domain to the PE domain before the Gly<sup>149</sup> maturation  
856 site, the remaining linker region is indicated in orange and the lipase domain is shown in grey. **B)**  
857 LipY with its PE domain highlighted in blue. **C)** LipY $\Delta$ PE where the removal of the PE domain is  
858 triggering a large opening of the active site. **D)** LipY $\Delta$ 149 without PE and linker region, allowing a  
859 better accommodation of the substrate without the catalytic pocket. **E)** LipY $\Delta$ 170 corresponding to  
860 the lipase domain only. The three-dimensional model structures of LipY, LipY $\Delta$ PE were from [14].  
861 LipY $\Delta$ 149 and LipY $\Delta$ 170 3D-model structures were generated with the automatic protein structure  
862 homology modeling server using the I-Tasser software program [81, 82] and the 4XVC PDB code  
863 [84] as template. The final model structures of LipY proteins were visualized using the PyMOL  
864 Molecular Graphics System (version 1.4, Schrödinger, LLC).

865

866 **Figure 3: Interfacial physico-chemical properties of LipY domains.** **A)** Adsorption of LipY,  
867 LipY $\Delta$ PE, LipY $\Delta$ 149 and LipY $\Delta$ 170 onto DOPG monomolecular films. Each enzyme (40 nM final  
868 concentration) was injected in aqueous phase (10 mM Tris-HCl buffer (pH 7.5) containing 150 mM  
869 NaCl) below the lipid film at various initial surface pressures ( $I_i$ ). The maximal surface pressure  
870 increase ( $\Delta I_{I_{\max}}$ ) was then recorded and plotted as a function of  $I_i$ . The critical surface pressure for  
871 penetration ( $I_c$ ; intercept of the linear regression with the  $x$ -axis) and  $\Delta I_0$  (intercept of the linear  
872 regression with the  $y$ -axis) were determined. Experiments were carried out in a cylindrical Teflon  
873 trough as described in the Materials and Methods section. Data are presented as mean values of two  
874 independent assays performed in duplicate (CV% < 5.0%). **B)** Temperature dependence of the  
875 wavenumber of the asymmetric methylene stretching  $\nu_{\text{as}}(\text{CH}_2)$  for DOPG in the absence and in the  
876 presence of LipY, LipY $\Delta$ PE, LipY $\Delta$ 149 and LipY $\Delta$ 170 at protein-to-lipid ratio of 1:10. Average

877 behavior of DOPG alone or in the presence of LipY $\Delta$ PE, LipY $\Delta$ 149 and LipY $\Delta$ 170 have been  
878 highlighted in thick black and compared to DOPG in the presence of LipY (filled blue dots).

879

880 **Figure 4: Investigation of LipY and its mutant form maturation processes through the Type**  
881 **VII secretion system of *M. marinum*.** **A)** Schematic representation of LipY and its mutant forms.  
882 The PE domain is highlighted in blue, the linker region before the Gly<sup>149</sup> maturation site is colored in  
883 green, the remaining linker region is colored in orange and the lipase domain is highlighted in grey.  
884 Specific point mutation (E92A and G149D) have been highlighted in red. **B)** Subcellular localization  
885 of cytoplasmic LipY<sup>E92A</sup>, LipY $\Delta$ 149 proteins and the exported MMAR\_0427 protein (which shares  
886 89% of identity with the monoglyceride lipase *M. tuberculosis* Rv0183 protein) were used as controls.  
887 Recombinant cells expressing 6 $\times$ His-tagged LipY proteins were treated with buffer containing (+) or  
888 not (-) Genapol<sup>®</sup>-X080 detergent. Pellet (P) and supernatant (S) fractions containing cytoplasmic and  
889 surface-exposed proteins, respectively, were separated by centrifugation. Samples were loaded onto  
890 12% SDS-PAGE and immunoblotted using HisProbe reagent. Grey arrows represented unprocessed  
891 forms whereas black arrows represented matured forms of the proteins. **C)** Subcellular localization  
892 of LipY, LipY<sup>G149D</sup>, PE-SGA-LipY $\Delta$ 149 and PE-SGA-LipY $\Delta$ 170 proteins in *M. marinum* by  
893 detergent extraction, as described above. **D)** Purification of the 6 $\times$ His-tagged mature form of PE-  
894 SGA-LipY $\Delta$ 170 proteins in *M. marinum* following detergent extraction and Ni-NTA affinity  
895 chromatography. Protein molecular weight and purity were assessed on 12% SDS-PAGE stained with  
896 Coomassie blue (CB) and further confirmed by western blotting (WB). Protein was loaded onto  
897 PVDF membrane, stained with Ponceau Red and N-terminal sequencing was performed. Analysis of  
898 LipY maturation process towards distinct recombinant forms of LipY. WT and PE-SGA-LipY $\Delta$ 170  
899 were confirmed by N-terminal sequencing whereas PE-SGA-LipY $\Delta$ 149 cleavage site remains  
900 putative. The maturation site is underlined and the SGA motif essential for LipY export is highlighted  
901 in red.

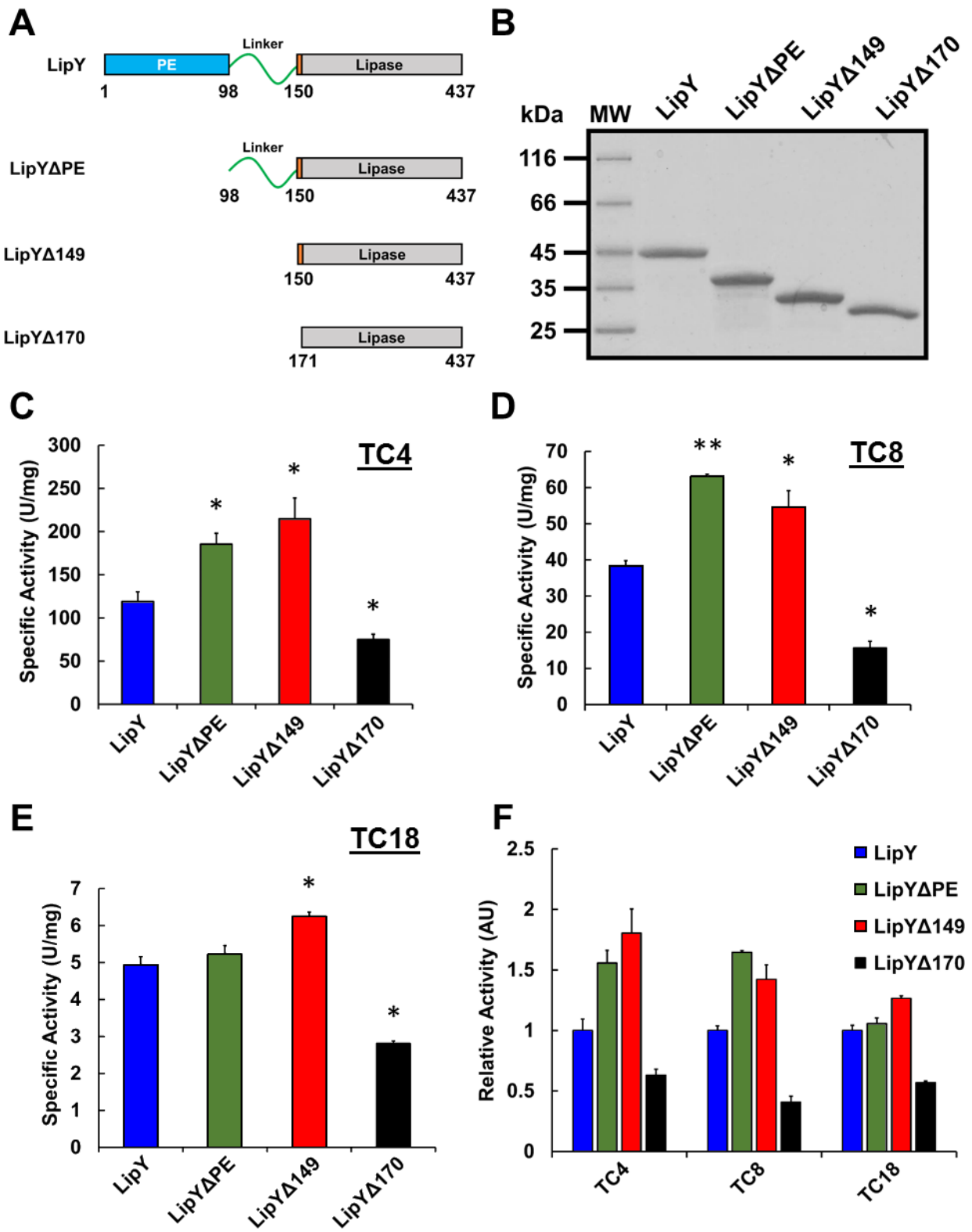
902

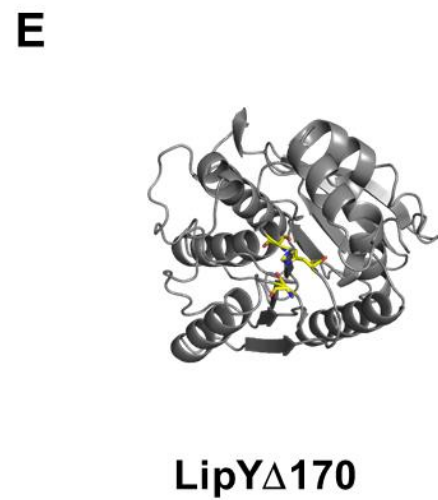
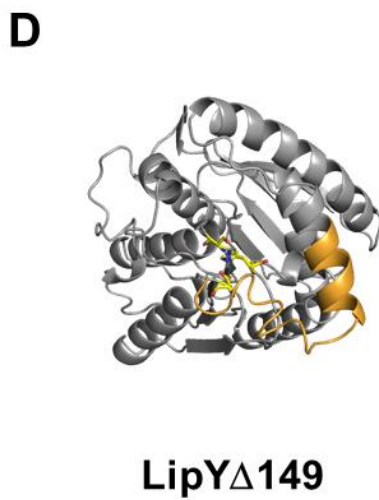
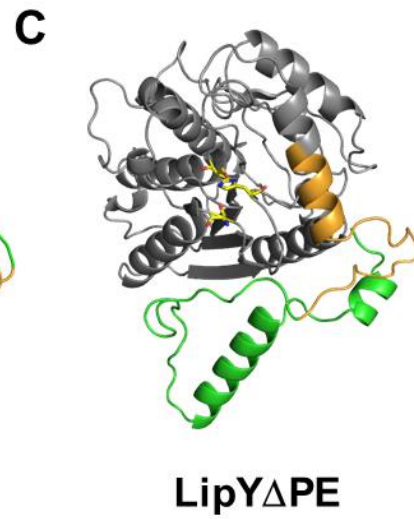
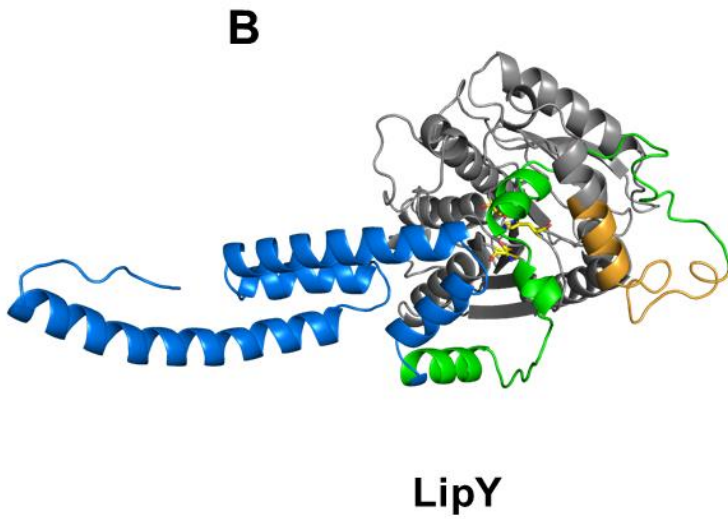
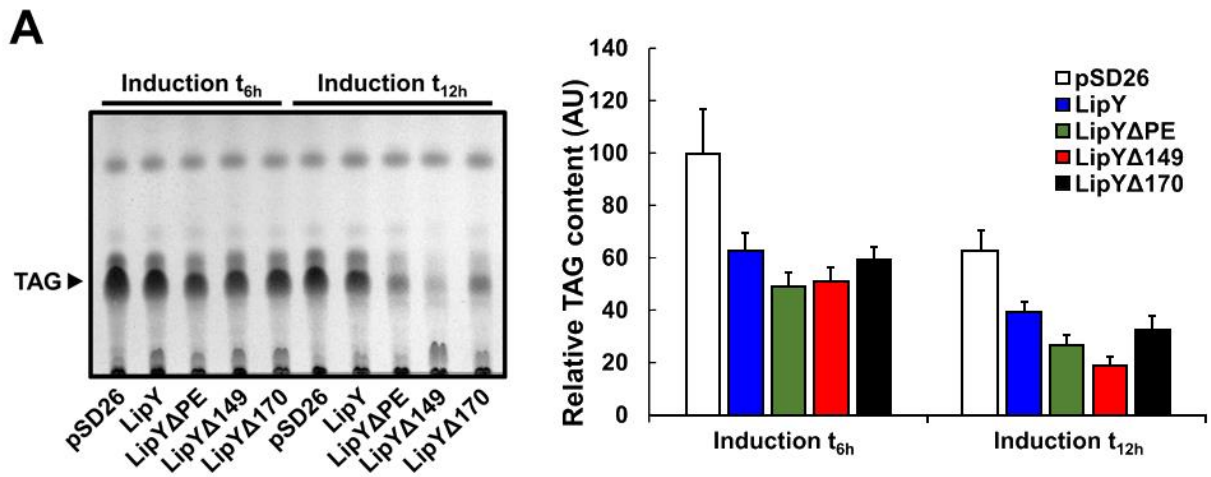
903 **Figure 5: Schematic representation of the contribution of LipY domains in ILI**  
904 **interaction/hydrolysis, secretion, maturation, and anchoring processes allowing host cell TAG**  
905 **breakdown.**

906 Upon infection the LipY protein is produced within the mycobacterial cytoplasm and possesses a dual  
907 localization. We proposed that during FFA acquisition, a weak portion of LipY remains in the  
908 cytoplasm in a full-length state, interacting either with the cytoplasmic membrane (1) or with the  
909 peripheral phospholipid layer of ILI (2) and that this interaction is mainly mediated by the PE domain  
910 (1-2). However, this N-terminal region also reduces the TAG-hydrolase activity of the lipase domain  
911 thus resulting in a slow breakdown of the neutral lipids contained within ILI (2). In the same time,  
912 the remainder of the protein is targeted to the ESX-5 machinery (3), and further recognized and  
913 matured by the MycP5 protease (4). This results in the formation of a mature truncated form of  
914 LipY variant (LipY $\Delta$ 149) that is anchored within the mycobacterial cell-wall (5). Deletion of the  
915 entire linker region did not affect this anchoring process suggesting that the lipase domain is  
916 responsible for the interaction within the mycomembrane (5). The truncated form LipY $\Delta$ 149, devoid  
917 of the PE domain and the first 53 amino acids of the linker, possesses a greater activity than the full-  
918 length protein (5) and contributes to FFA acquisition by hydrolyzing host cell TAG within the  
919 phagosomal lumen of foamy macrophages (5). The red star corresponds to a schematic representation  
920 of the catalytic serine within the lipase domain. CM: cytoplasmic membrane; PG: peptidoglycan, AG:  
921 arabinogalactan; MA: mycolic acids; DAG: diacylglycerol; MAG: monoacylglycerol; TAG:  
922 triacylglycerol; FFA: free fatty acid.

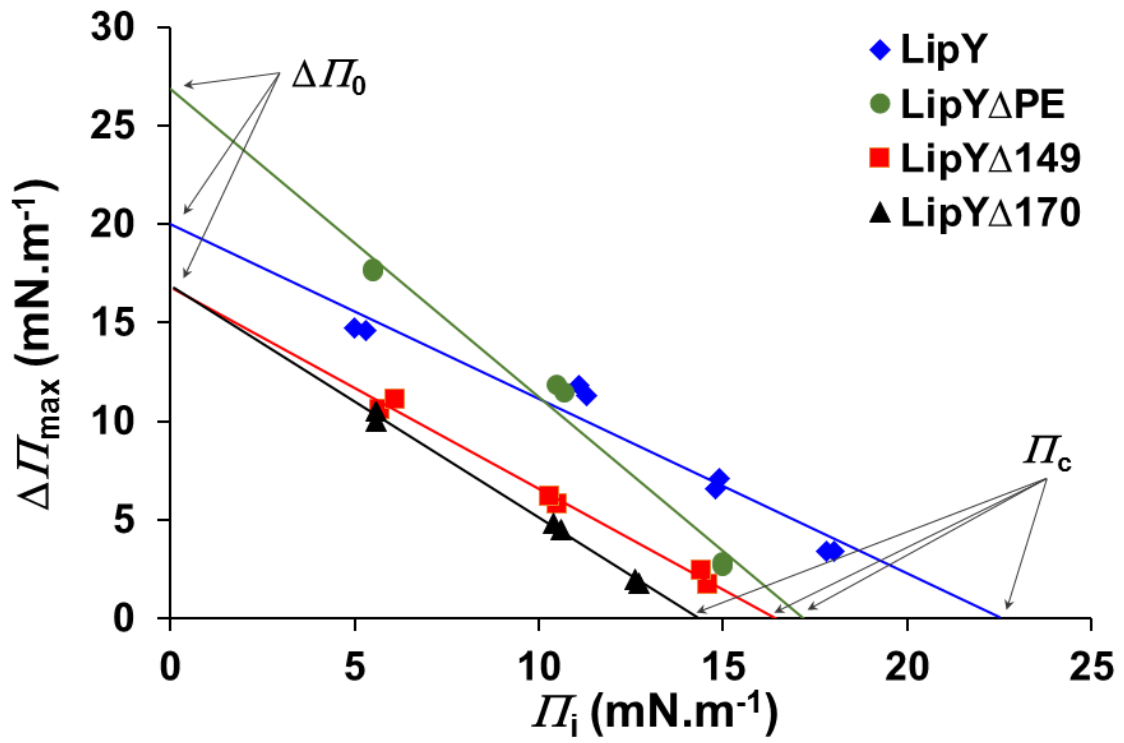
923

924

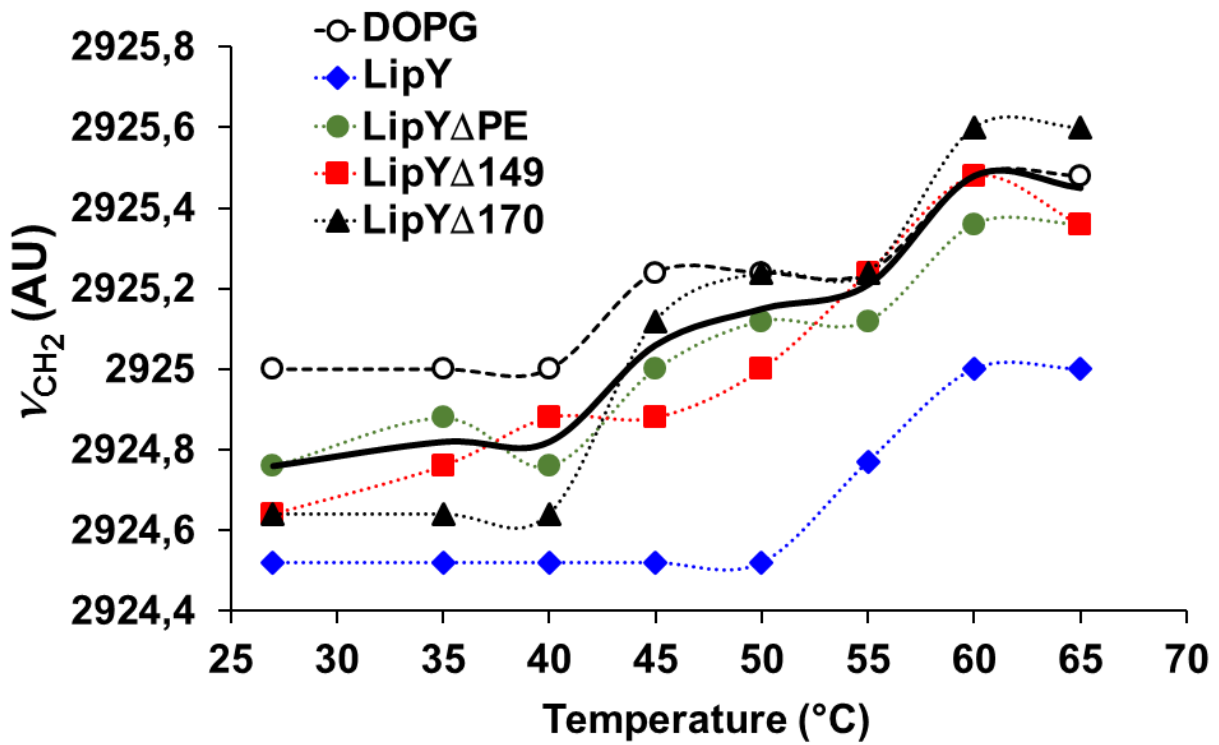




**A**



**B**



933

934

935

